

**NAVAL POSTGRADUATE SCHOOL**  
**Monterey, California**



**THESIS**

**AN EXPERIMENTAL INVESTIGATION OF FLAPPING  
WING PROPULSION FOR MICRO AIR VEHICLES**

by

Sean Joseph Duggan

June 2000

Thesis Advisor:  
Co-Advisor:

Kevin D. Jones  
Max F. Platzer

Approved for public release; distribution is unlimited.

DTIC QUALITY INSPECTED 4

20000825 023

# REPORT DOCUMENTATION PAGE

Form Approved  
OMB No. 0704-0188

Public reporting burden for this collection of information is estimated to average 1 hour per response, including the time for reviewing instruction, searching existing data sources, gathering and maintaining the data needed, and completing and reviewing the collection of information. Send comments regarding this burden estimate or any other aspect of this collection of information, including suggestions for reducing this burden, to Washington headquarters Services, Directorate for Information Operations and Reports, 1215 Jefferson Davis Highway, Suite 1204, Arlington, VA 22202-4302, and to the Office of Management and Budget, Paperwork Reduction Project (0704-0188) Washington DC 20503.

1. AGENCY USE ONLY (Leave blank)		2. REPORT DATE June 2000		3. REPORT TYPE AND DATES COVERED Master's Thesis	
4. TITLE AND SUBTITLE An Experimental Investigation of Flapping-Wing Propulsion for Micro Air Vehicles				5. FUNDING NUMBERS	
6. AUTHOR(S) Sean Joseph Duggan					
7. PERFORMING ORGANIZATION NAME(S) AND ADDRESS(ES) Naval Postgraduate School Monterey, CA 93943-5000				8. PERFORMING ORGANIZATION REPORT NUMBER	
9. SPONSORING / MONITORING AGENCY NAME(S) AND ADDRESS(ES)				10. SPONSORING/MONITORING AGENCY REPORT NUMBER	
11. SUPPLEMENTARY NOTES The views expressed in this thesis are those of the author and do not reflect the official policy or position of the Department of Defense or the U.S. Government.					
12a. DISTRIBUTION / AVAILABILITY STATEMENT Approved for public release; distribution is unlimited.				12b. DISTRIBUTION CODE	
13. ABSTRACT (Maximum 200 words) Flapping-wing propulsion is studied experimentally through thrust measurements and flow visualization. The objective of the research is to provide further insight into the aerodynamics of flapping-wing micro air vehicles (MAVs). Experimental work is conducted in the NPS 1.5 m x 1.5 m in-draft wind tunnel. A previously constructed model is suspended by thin wires and is used to measure the thrust performance of the flapping-wing MAV. For this experiment, the model is tested in four configurations; three with varying wing mount stiffness and the fourth with an articulated pitch mechanism. Thrust is indirectly determined using a laser range-finder to measure stream-wise displacement of the model. Three methods of flow visualization are attempted to gain further insight into the flow-field around the MAV. First tufts are placed on and around the model to identify the flow-field. Second, a smoke rake placed outside the tunnel is used to route smoke into the test section. Thirdly, a smoke wire system is used to produce smoke in the test section. Experimental results are compared with flow visualization results and previous experimental and numerical work.					
14. SUBJECT TERMS Flapping-wing, Micro Air Vehicle, Low Reynolds Number, Flow Visibility				15. NUMBER OF PAGES 74	
				16. PRICE CODE	
17. SECURITY CLASSIFICATION OF REPORT Unclassified	18. SECURITY CLASSIFICATION OF THIS PAGE Unclassified	19. SECURITY CLASSIFICATION OF ABSTRACT Unclassified		20. LIMITATION OF ABSTRACT UL	

NSN 7540-01-280-5500

Standard Form 298 (Rev. 2-89)  
Prescribed by ANSI Std Z39-18

THIS PAGE INTENTIONALLY LEFT BLANK

**Approved for public release; distribution is unlimited**

**AN EXPERIMENTAL INVESTIGATION OF FLAPPING WING PROPULSION FOR  
MICRO AIR VEHICLES**

Sean Joseph Duggan  
Captain, Canadian Armed Forces  
B.Eng., Royal Military College of Canada, 1995

Submitted in partial fulfillment of the  
requirements for the degree of

**MASTER OF SCIENCE IN AERONAUTICAL ENGINEERING**

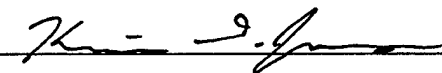
from the


**NAVAL POSTGRADUATE SCHOOL  
June 2000**


Author:

  
Sean Joseph Duggan

Approved by:

  
Kevin D. Jones, Thesis Advisor

  
Max F. Platzer, Co-Advisor

  
Max F. Platzer, Chairman  
Department of Aeronautics and Astronautics

THIS PAGE INTENTIONALLY LEFT BLANK

## ABSTRACT

Flapping-wing propulsion is studied experimentally through thrust measurements and flow visualization. The objective of the research is to provide further insight into the aerodynamics of flapping-wing micro air vehicles (MAVs). Experimental work is conducted in the NPS 1.5 m x 1.5 m in-draft wind tunnel. A previously constructed model is suspended by thin wires and is used to measure the thrust performance of the flapping-wing MAV. For this experiment, the model is tested in four configurations; three with varying wing mount stiffness and the fourth with an articulated pitch mechanism. Thrust is indirectly determined using a laser range-finder to measure stream-wise displacement of the model. Three methods of flow visualization are attempted to gain further insight into the flow-field around the MAV. First tufts are placed on and around the model to identify the flow-field. Second, a smoke rake placed outside the tunnel is used to route smoke into the test section. Thirdly, a smoke wire system is used to produce smoke in the test section. Experimental results are compared with flow visualization results and previous experimental and numerical work.

THIS PAGE INTENTIONALLY LEFT BLANK

## TABLE OF CONTENTS

I.	INTRODUCTION.....	1
A.	OVERVIEW.....	1
B.	BACKGROUND.....	1
C.	FLAPPING-WING PROPULSION.....	2
II.	EXPERIMENTAL ANALYSIS .....	5
A.	EXPERIMENTAL APPARATUS .....	5
1.	MAV Construction.....	5
2.	Wind Tunnel.....	6
3.	Miscellaneous Equipment .....	7
B.	EXPERIMENTAL CONFIGURATIONS .....	9
C.	EXPERIMENTAL METHOD .....	10
D.	EXPERIMENTAL DATA REDUCTION.....	13
E.	EXPERIMENTAL RESULTS AND ANALYSIS .....	17
1.	Experimental Results .....	17
2.	Error Analysis .....	22
III.	FLOW VISUALIZATION.....	25
A.	FLOW VISUALIZATION METHODS .....	25
1.	Smoke Rake and Fog Machine.....	25
2.	Tell-Tale Tufts.....	26
3.	Smoke Wire System .....	26
B.	FLOW VISUALIZATION RESULTS .....	29
1.	Tell -Tale Tufts.....	29
2.	Smoke Wire System .....	30
IV.	CONCLUSIONS.....	41
V.	RECOMMENDATIONS .....	43
	APPENDIX A. MATLAB PROGRAM FOR DSO-2102 OSCILLOSCOPE DATA REDUCTION.....	45
	APPENDIX B. THREE DIMENSIONAL PLOTS OF EXPERIMENTAL DATA.....	53
	LIST OF REFERENCES .....	57
	INITIAL DISTRIBUTION LIST.....	59



## LIST OF SYMBOLS

$AR$	aspect ratio, $b^2/S$
$b$	effective wing span
$b^*$	total wing span
$c$	chord length
$C_d$	drag coefficient per unit span, $D/(q_\infty c)$
$C_D$	drag coefficient, $D/(q_\infty S) = C_d b$
$C_p$	power coefficient, $\text{power}/(q_\infty S V_\infty) = -C_l \dot{y} - C_m \dot{\alpha}$
$C_t$	thrust coefficient, $T/(q_\infty S)$
$D$	drag
$f$	oscillation frequency in Hz
$f_m$	pendulum frequency of installed swinging model
$g$	acceleration due to gravity
$h_y$	vertical plunge amplitude in terms of $c$
$k$	reduced frequency, $2\pi f c/V_\infty$
$L$	effective pendulum length
$q_\infty$	free-stream dynamic pressure, $\frac{1}{2} \rho_\infty V_\infty^2$
$S$	wing area, $bc$
$t$	time
$T$	thrust
$V_\infty$	free-stream velocity
$x_p$	pivot location from leading edge in terms of $c$
$y$	vertical displacement in terms of $c$
$\alpha$	angle of attack (AOA)
$\alpha_{eff}$	effective angle of attack
$\alpha_{geom}$	geometric angle of attack
$\alpha_{ind}$	induced angle of attack
$\Delta\alpha$	sinusoidal pitch amplitude
$\phi_y$	phase difference between pitch and vertical plunge
$\eta_t$	propulsive efficiency, $C_t/C_p$
$\lambda$	taper ratio, $c_t/c_0$
$\Lambda$	sweep angle
$\rho_\infty$	free-stream air density
$\tau$	non-dimensional time, $tV_\infty/c$
$\omega$	circular frequency, $2\pi f$
$(\dot{\phantom{x}})$	rate of change w.r.t. $\tau$

## **ACKNOWLEDGEMENT**

The author would like to extend his sincere appreciation to Dr. Kevin Jones for his patient instruction, technical advice and guidance and Professor Max Platzner for his oversight and encouragement.

THIS PAGE INTENTIONALLY LEFT BLANK

## **I. INTRODUCTION**

### **A. OVERVIEW**

In this paper the effects of wing mount stiffness on the aerodynamic performance of a flapping-wing Micro Air Vehicle (MAV) was investigated. In addition, flow visibility methods were utilized in an attempt to gain further knowledge of the flow field about the MAV. While there are many potential propulsive methods for MAVs, including conventional or rotary wing designs, this paper builds upon previous research conducted at NPS to increase the knowledge base of the flapping-wing propulsion system for the MAV application.

The experimentation for this paper was conducted in the NPS 1.5 m x 1.5 m in-draft wind tunnel using a previously developed parallel flapping-wing MAV. To obtain thrust data, the MAV was suspended with wire from the roof of the tunnel with thrust indirectly measured using a laser rangefinder to measure the streamwise displacement of the MAV.

### **B. BACKGROUND**

With a shift towards more diverse military operations in recent years, an operational need for locally owned and operated reconnaissance assets has been identified. The recent development of new technologies such as micro-electromechanical systems (MEMS), tiny CCD-array cameras, equally small infrared sensors and chip-sized hazardous substance detectors has made the development of small airborne reconnaissance vehicles viable. To this end, the Defense Advanced Research Projects Agency (DARPA) is funding research into the development of MAVs. A MAV is defined by DARPA as "an affordable, fully functional, militarily capable, flight vehicle, limited to 15 cm in length, width or height." [Ref. 1]. These vehicles must be able to stay aloft for 20 to 60 minutes, cover a distance of up to 10 km and carry a payload weighing up to 20 grams. The flight regime in which MAVs will fly, is for the most part

unstudied. The low Reynolds number flight, which will be encountered by MAVs, has been up until this point, strictly the domain of insects and small birds.

Essential to the success of a MAV design is the requirement for high-density propulsion and power sources to fulfill the MAV's propulsive requirements. Previous research indicates that a parallel flapping-wing may produce higher propulsive efficiency than a conventional propeller driven or rotary winged vehicle in low Reynolds number flow. The research summarized in this paper builds upon previous research conducted in the study of flapping-wing MAVs.

### C. FLAPPING-WING PROPULSION

In 1909 and 1912, Knoller [Ref. 2] and Betz [Ref. 3] respectively, independently observed that a flapping-wing creates an effective angle of attack,  $\alpha_e$ , resulting in a normal force vector with both lift and thrust components. The Knoller-Betz effect is illustrated in Figure 1.

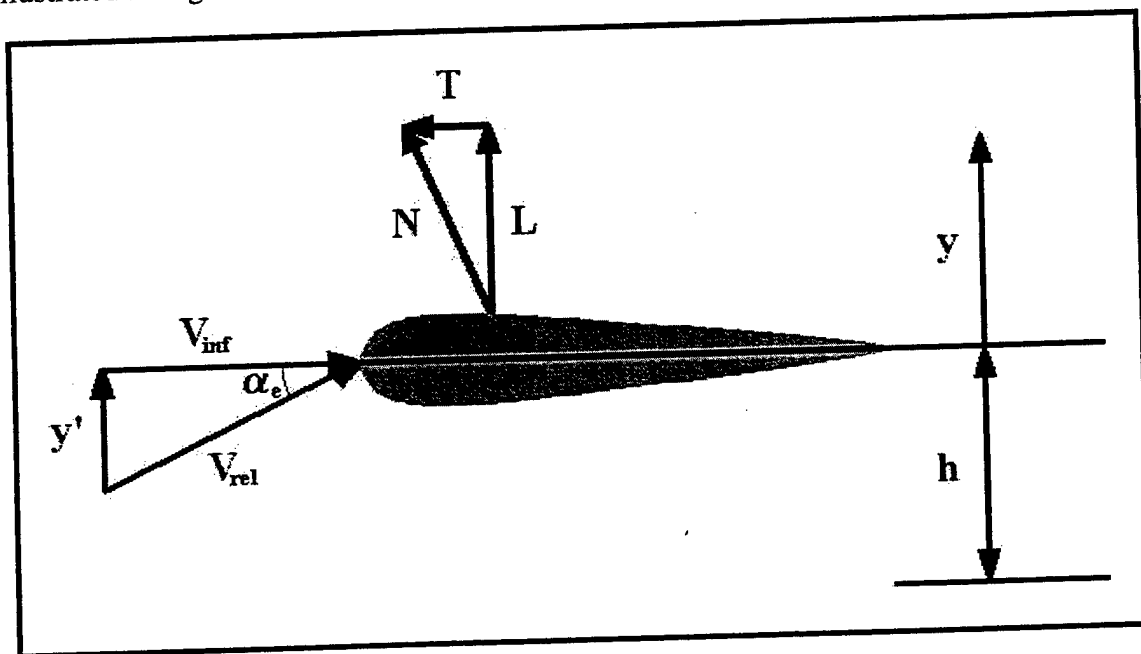


Figure 1. Effective Angle of Attack Produced by Flapping-Wing.

In 1922, Katzmayer [Ref. 4] demonstrated the Knoller-Betz effect experimentally by measuring an average thrust with a stationary wing in a sinusoidally oscillating wind stream. This field of research was further advanced in 1924 when Birnbaum [Ref. 5 & 6] observed the conditions that lead to flutter or the generation of thrust and suggested a flapping-wing as an alternative to the conventional propeller. Over the next few decades, much research was conducted on the aerodynamics of flutter and gust response. However, it wasn't until the mid-1930s that further research was conducted by von Kármán and Burgers [Ref. 7], to explain the theory behind the generation of thrust or drag in a flapping-wing. For a more detailed history of flapping-wing research refer to Refs. 8 & 10.

More recently, numerical and experimental work was conducted by Jones and Platzer [Ref. 8]. In their research, they found that the two-airfoil, opposed-plunge configuration was the configuration which appeared most promising for the MAV application due to this configuration's relatively high propulsive efficiency and the inherent stability resulting from the opposed plunge motion. In this application, the lower airfoil acts as an image airfoil in a ground-effect analysis. The opposed plunge configuration is shown in Figure 2.

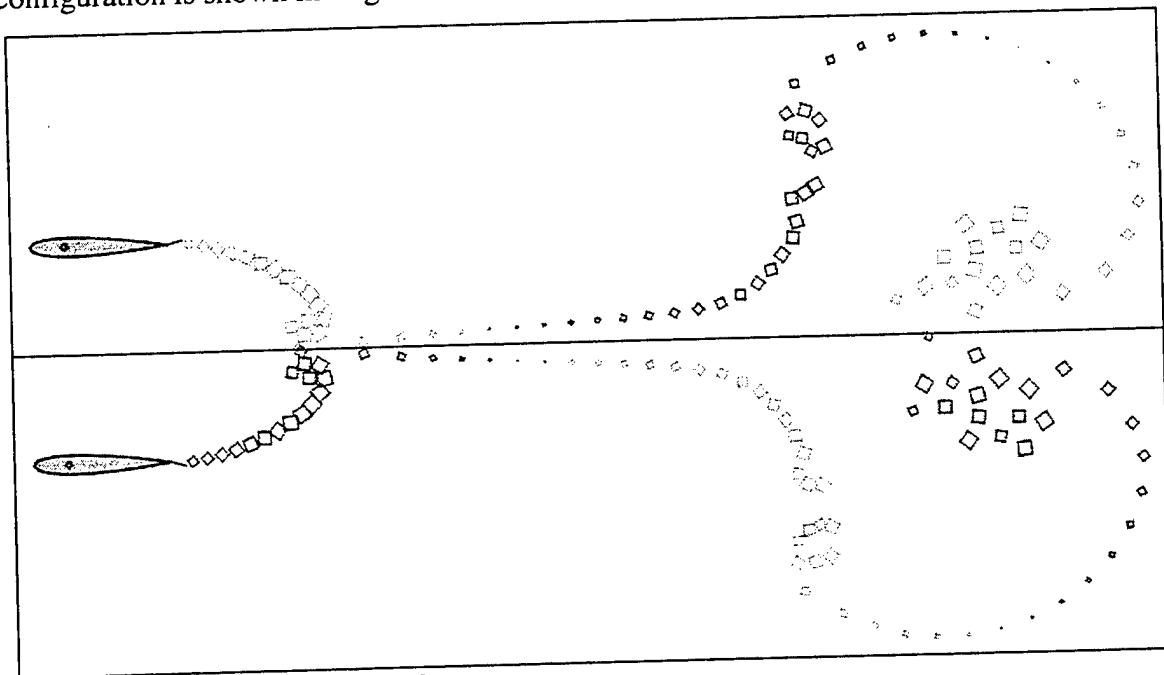


Figure 2. Airfoil in Ground Effect.

When operating in ground effect, downwash velocities are decreased. The ground presents a boundary condition requiring the normal component of velocity to go to zero altering the streamline pattern around the airfoil. In an analytic ground-effect analysis, a mirror image of the airfoil is placed across the plane of symmetry. The vortex system of this image airfoil is opposite the original system. In order to satisfy the boundary condition, the vertical velocities induced by these two image vortex systems will cancel at the plane of symmetry. In addition to vertical velocity going to zero, the destructive interference of the counter-rotating vortex systems diminishes the influence of the trailing vortices on the airfoil.

The parallel flapping-wing configuration studied in this paper approximates the beneficial aspects of ground-effect when flying out of ground-effect. In this three-dimensional case, the reduced influence of the tip vortices, lessen the induced angle of attack, increasing lift and thrust.

## II. EXPERIMENTAL ANALYSIS

### A. EXPERIMENTAL APPARATUS

#### 1. MAV Construction

The MAVs used in this research were constructed by Dr Kevin Jones [Ref. 10]. A side view of the MAV with the articulated pitch mechanism can be seen in Figure 3. The MAV is designed around an exceptionally small, geared stepping motor from RMB Smoovy. The motors are 5mm in diameter with the 25:1 planetary gear system, are approximately 25mm long and weigh a mere 2.4g. These motors produce about  $2.5 \times 10^{-3}$  Nm of torque at speeds up to 800 RPM.

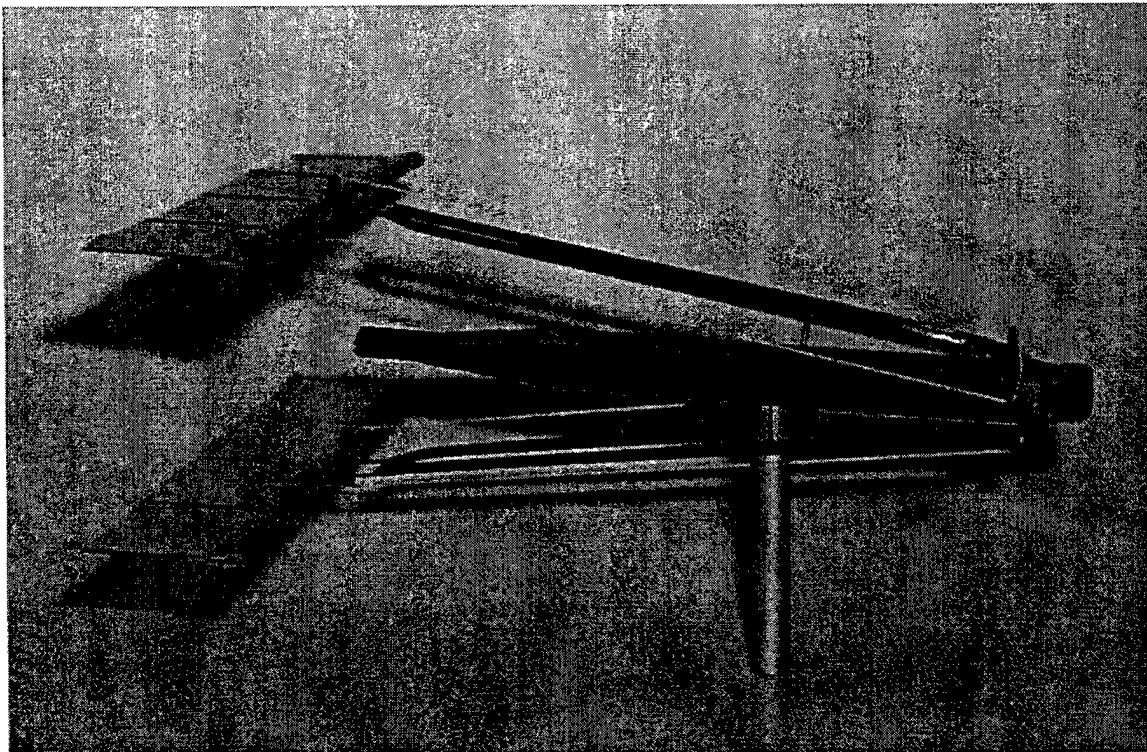


Figure 3. MAV with Articulated Pitch.

The brushless motors are controlled by an oscillatory driver circuit, which allows for very precise, steady and reproducible rotational speeds. As the control circuit and power supply are large and bulky, they are currently mounted external to the model.



Three-pole power is fed to the model through four 0.076mm diameter copper wires which support the model. The support wires connect to the model via small gold plated pins, at the nose and near the tail of the model. The mass of the wires is negligible compared to the mass of the model and they are flexible enough so as not to impede the model's motion.

The model's body has composite construction, built primarily out of balsa wood and very thin graphite-epoxy laminates. The motor is connected by thin-wall silicon tubing to a crankshaft that moves the flapping beams via Scotch yokes constructed of piano wire. The wing's leading edge is a teardrop shaped piece of balsa wood with carbon-fiber ribs running to the trailing edge of the Japanese tissue wing surface. In this paper, the wings had a span of 150mm and a chord of 35mm.

The wings are super-glued to the flapping beams using thin carbon fiber strips whose length and width control the elasticity of the joint. The elasticity of the wing mount allows for a passive feathering mechanism. The wing deflects in pitch proportionally to the moment about its leading edge. In this paper, the elasticity of the wing joint was adjusted by decreasing the distance between the wing's leading edge and the flapping beam. Three different distances were used for the tested model. In addition, an active pitch control was added to the model by gluing arms and strings to the model's body and wings to achieve a pure plunge motion for the wing. The four configurations were tested in the NPS low-speed in-draft smoke tunnel and the results compared.

## **2. Wind Tunnel**

Experiments were performed in the NPS low-speed in-draft smoke tunnel depicted in Figure 4. The tunnel was modeled after the smoke tunnel of the Naval Air Engineering Lab in Philadelphia [Ref. 12]. Air is ingested from inside the building through a square 4.5 x 4.5 m inlet, converging through a 9:1 bell shaped contraction to a 1.5 x 1.5 m test section. Tunnel speed is controlled by a variable pitch fan driven by a constant speed electric motor. Motor and fan vibration are isolated from the test section by rubber sleeves on each side of the motor/fan assembly. The tunnel velocity range is 0 to 9.5 m/s.

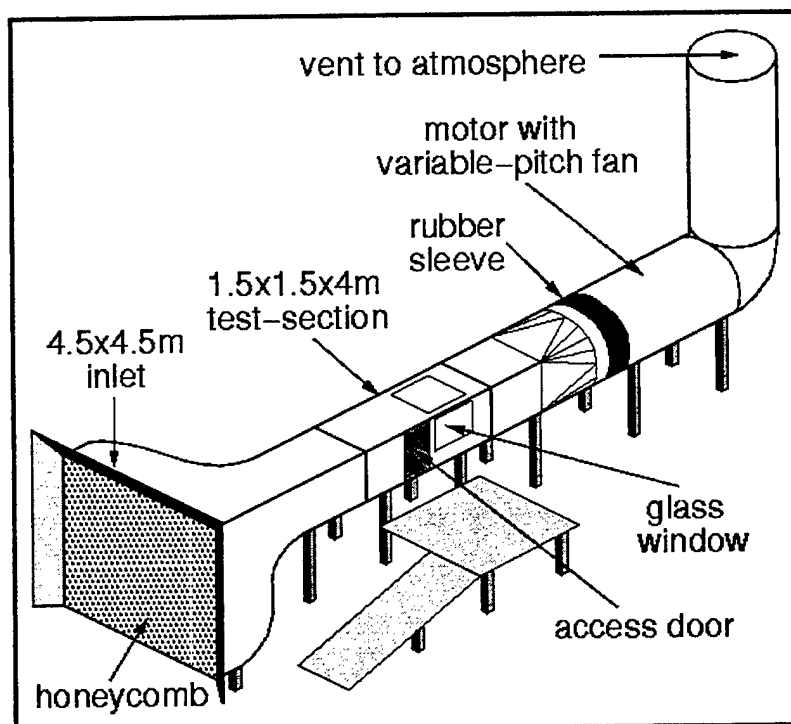


Figure 4. NPS Low-Speed In-draft Wind Tunnel.

Late in 1999, Lt Tim Lund rebuilt the neglected wind tunnel [Ref. 11]. His extensive repairs included fixing the fan, resetting the variable pitch fan blades to achieve lower velocities, removed old fixtures, refinished the tunnel floor and the old pitot-static system was replaced. A tunnel calibration was performed using LDV following tunnel repairs and was used in the reduction of the data for this paper. In addition, the test section turbulence intensity level was determined and remained below 1.75% with tunnel velocities over 1.5 m/s [Ref. 11].

### 3. Miscellaneous Equipment

A pitot-static tube located approximately two feet below and one foot upstream of the model was used to determine the tunnel velocity. The pitot-static tube was connected to a MKS Baratron type 223B differential pressure transducer. The transducer voltage output, which is linear with pressure, was read by a Metex 3610D digital multimeter that linked the voltage data to a PC for recording.

A frequency strobe light was used to set the flapping-wing frequency. The strobe was set to the desired frequency, and the wing frequency adjusted to match. The accuracy of the strobe was checked using a Monarch Instrument Tach IV Digital Optical Tachometer. Strobe error varied with frequency to a maximum of 1.5 percent in the frequencies of interest. Actual frequency used for data reduction was determined after the experiment using voltage data from the model controller.

A Matsushita Electric Works Model ANL1651AC laser rangefinder was used to determine model displacement when flapping. The sensor accuracy as prescribed by the manufacturer is  $\pm 100\mu\text{m} \pm 0.002 \times \Delta x$  for the range  $130\text{mm} \pm 35\text{mm}$ . Its measurable range is 8 – 18 cm, with accuracy decreasing with increased distance from the center point. The rangefinder was positioned behind the model at its center point distance of 13 cm. During runs, this corresponded to a position 3 to 4 chord lengths behind the model and was not thought to create a significant flow interference effect. The output of the rangefinder is 1 V/cm displacement.

A Link Instruments DSO-2102 digital storage oscilloscope was used to measure voltage. The DSO-2102 was connected to a desktop PC for display and recording of the voltage signals. The oscilloscope simultaneously records two data channels. One channel was designated for the laser rangefinder, and this data was subsequently used to determine thrust. The second channel was used to collect controller voltage data for eventual determination of flapping frequency and to synchronize data. The oscilloscope features 32 kilobyte buffers per channel.

A Setra EL410D digital balance was used to measure the mass of the model before each run. The scale has an accuracy of  $\pm 0.001\text{g}$ . The model's mass was found to vary by as much as 0.005g from day to day, due to humidity, dust or other environmental contamination. A Rosco model 4500 smoke generator was used for flow visibility. A smoke rake was constructed to match the output of the smoke generator.

A Sony DCR-VX1000 digital Video camera was used to capture video images of the MAV in motion. Using the manual focus, auto exposure, a shutter speed of 1/8 sec and the strobe light set at approximately 12 Hz (just slightly faster than the MAV

flapping frequency), acceptable video images of the MAV were obtained. Capturing flow visualization images using the smoke rake or smoke wire proved to be more difficult. A Kodak DC 260 digital camera was used to capture flow visualization images (thread tell-tales). Best results were achieved by setting the manual focus to 18 inches, the exposure to 0.5 sec (the slowest manual timed exposure) and the strobe light and MAV flapping frequency set to approximately 8 Hz. This configuration lead to some blurring as approximately 4 cycles were captured per image.

## B. EXPERIMENTAL CONFIGURATIONS

Wing Span	$b^*$	150 mm
Wing Chord	C	35 mm
Aspect Ratio	$AR=b^2/S=b/c$	4.29
Taper Ratio	$\lambda=c_t/c_o$	1
Sweep Angle	$\Lambda$	$0^\circ$
Velocity	$V_\infty$	0 - 6 m/s
Flapping Frequency	$F$	8, 10, 12, 14 Hz (approximate)
Mean Wing Separation	$\Delta y_m$	$0.8429c$
Plunge Amplitude	H	25.4 mm
Reduced Frequency	K	$0.29 - \infty$

Table 1. General Experimental Configuration.

Wing Stiffness (Low)	K	$4.746 \times 10^{-3} \text{ Nm}$
Wing Stiffness (Medium)	K	$6.384 \times 10^{-3} \text{ Nm}$
Wing Stiffness (High)	K	$14.17 \times 10^{-3} \text{ Nm}$
Wing Stiffness (Articulated Pitch)	K	N/A

Table 2. Wing Mount Stiffness.

### C. EXPERIMENTAL METHOD

Before each wind tunnel run, the model with mounting pins was weighed using the Setra scale. The model was then hung in the wind tunnel with four 0.076mm diameter copper wires and mounting pins as can be seen in Figure 5. After the model was installed in the tunnel the laser rangefinder was positioned near its zero voltage center point, 13 cm behind the model. The DSO program was then started on the PC and setup to record data at 1 KHz (approximately 32 sec of data). The model was given a push, and once the displacement fell within the limits (500 mV/division, 10 divisions) displayed in the DSO program ( $\pm 2.5$  cm), data recording began. Three separate sets of data were taken before either the tunnel or the model was turned on. This data was used to determine both the effective pendulum length for thrust calculations and the model's initial position. A close-up image of the MAV in motion with laser can be seen in Figure 6.

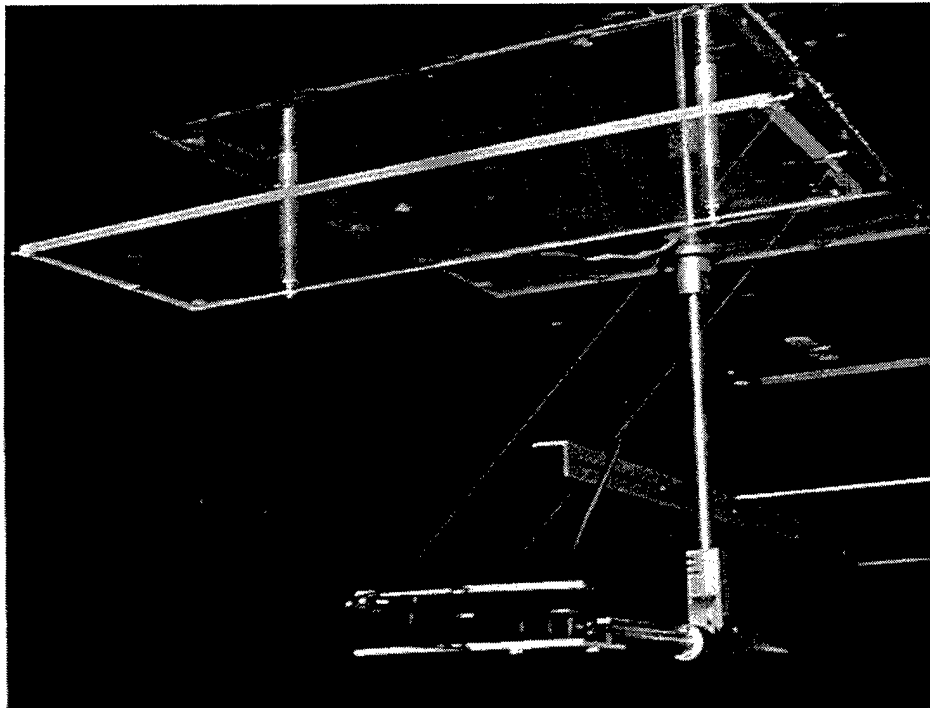


Figure 5. MAV Installed in Tunnel.

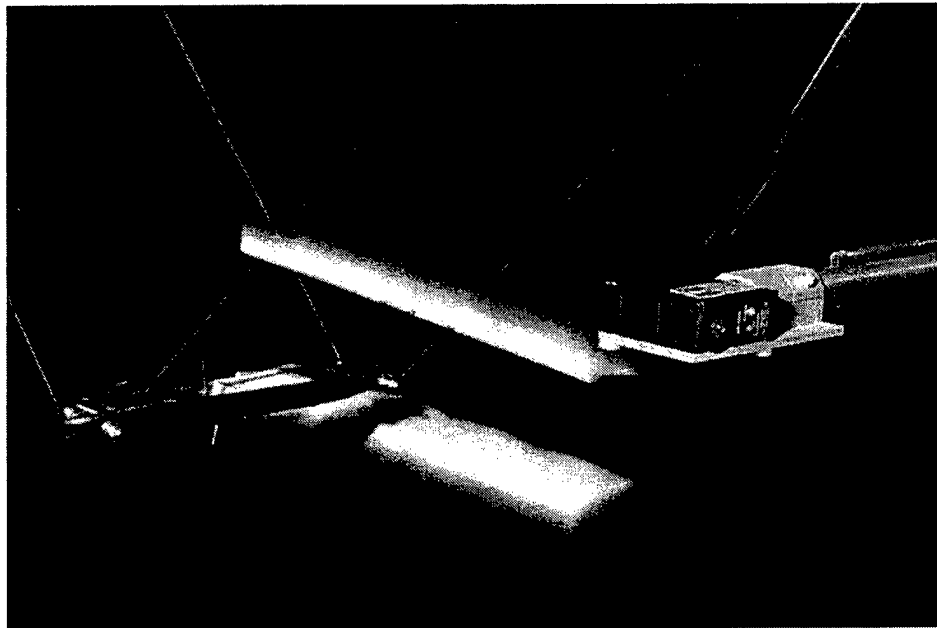


Figure 6. MAV in Motion and Laser.

Before any thrust measurements were taken, a 60-second sample of pitot-static data (sample rate of 1 Hz) was taken to establish a zero velocity voltage. This data was recorded on the PC using the software provided with the Metex 3610D DMM.

Next, a set of thrust measurements were taken with the tunnel off. With the controller mode selector knob in the variable speed position, the power was turned on. The default power setting for this start-up mode was set so that the model's wings would be flapping at approximately 8 Hz. The strobe was set to 8 Hz to verify the flapping frequency. In order to record frequency data, the TTL output from the controller was connected to the DSO. With the 25:1 gearbox installed in the model, 25 voltage pulses from the controller correspond to one complete cycle for the model. Once the model position stabilized, recording of the position data by the DSO program, set to sample at 10 KHz, was started. Once again, three sets of data were recorded at each frequency.

The strobe frequency was then increased in 2 Hz increments up to 14 Hz. At each 2 Hz increment, the signal to the MAV was stepped up until the flapping frequency matched the strobe or the motor stalled. The motor tended to stall if the load became too great or the MAV was disturbed by an external disturbance.

Once the static measurements were complete, the wind tunnel was turned on. Initially, the pitch on the fan blades was set to give zero tunnel velocity. The pitch was slowly increased incrementally to the velocity of interest. Once the velocity stabilized, 60-seconds of pitot-static data was recorded on the PC (1 Hz sample rate).

As the focus of this paper is on determining the feasibility of using a flapping-wing mechanism to generate thrust, the drag of the MAV is required so that the gross thrust generated by the MAV can be determined. As the drag of the MAV varies with wing position (maximum drag when wings are together), the wings were flapped at an extremely low frequency, on the order of 0.1 Hz, to determine an average drag. The DSO was used to record the position data from the laser rangefinder at 1 KHz sample rate. Again three sets of data were taken. The position data from the DSO for the stiff wing mount run at approximately 5 m/s and 0.1 Hz can be seen in Figure 7.

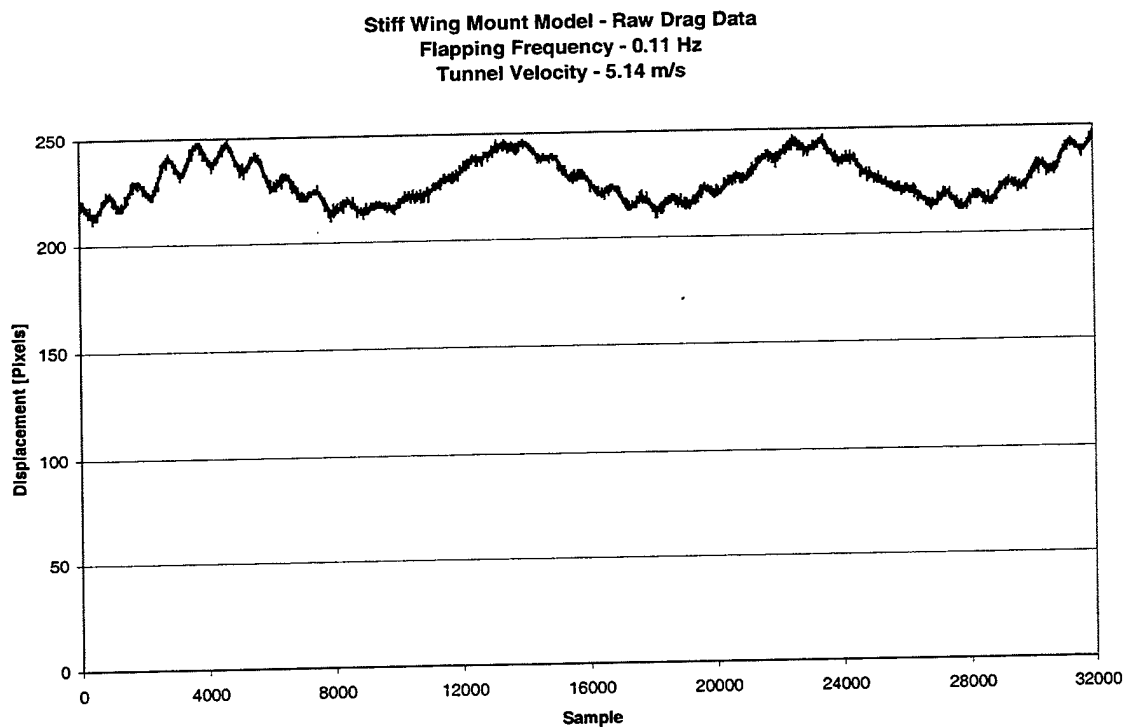


Figure 7. Change in MAV Drag with Wing Position.

Once the drag data had been recorded, thrust measurements were taken as per the static case at 8, 10, 12 and 14 Hz (if the motor allowed). Once the measurements were

made, the tunnel speed was increased until a tunnel speed of 5 to 6 m/s was reached. At tunnel speeds in this range, the model's drag displaced it sufficiently to force the displacement data outside the display limits of the DSO software. With tunnel speeds from 0 – 5.9 m/s and flapping frequencies from 8 - 14 Hz reduced frequencies in the range  $k = 0.29 - \infty$  were observed.

#### D. EXPERIMENTAL DATA REDUCTION

At each test point, three different sets of data were recorded; voltage from the differential pressure transducer, output from the controller and voltage data from the laser rangefinder. To reduce the pressure transducer data to velocity [m/s], Equation 1, obtained from an LDV- calibration completed by Lt Lund [Ref. 11], was used.

$$Vel = 0.4819(mV)^{0.489} \quad (1)$$

The pressure data file was opened in Excel and converted to velocities using Equation 1. The average and standard deviation of the 60-second sample were then taken. To account for changing environmental conditions, an initial and final pressure transducer reading were taken. A linear change in the zero condition was assumed and the difference between the initial and final condition was divided by the number of velocities and added to each velocity reading. The test velocities ranged from 0 – 5.9 m/s. To determine the model's effective pendulum length for thrust calculations and the model's initial position, the 32-second (1 Hz sample rate) static swing data file was opened in Excel and the model's displacement was plotted versus sample number (see Figure 8).



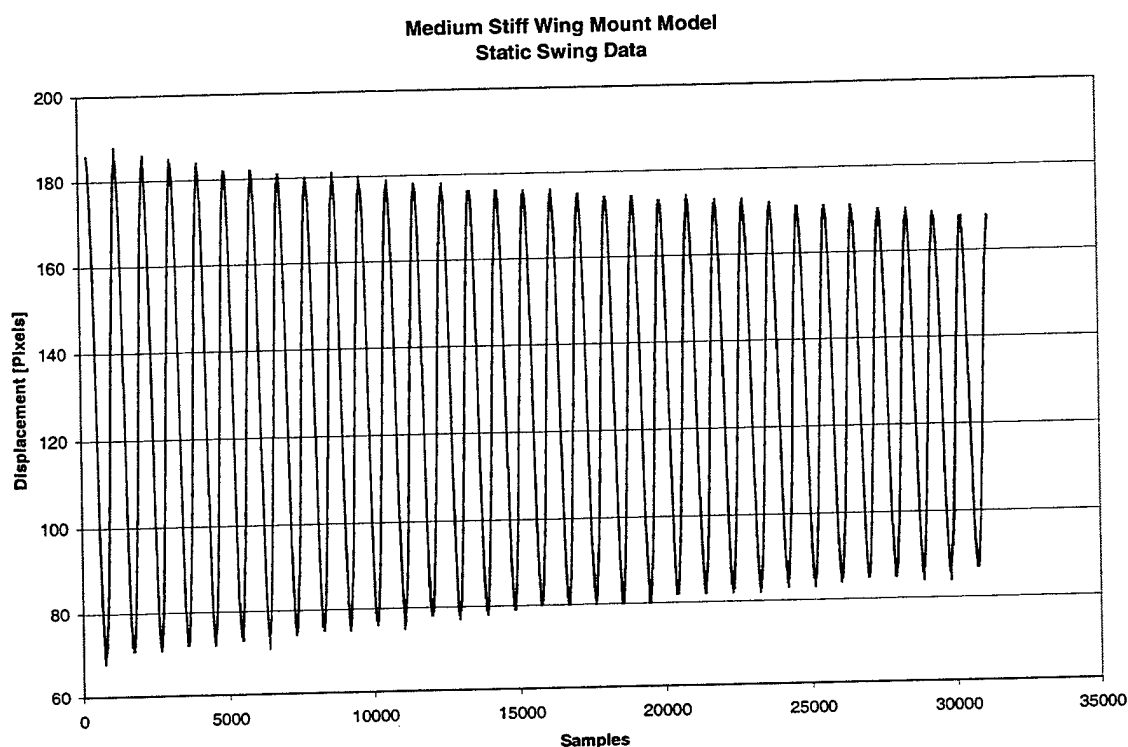


Figure 8. MAV Displacement vs Sample #.

Next, the data was edited so that an integer number of cycles were represented. The number of cycles and the number of samples within the cropped data set were counted and the frequency of the hanging model was determined. The installed model's frequency,  $f_m$ , was approximately 1.07 Hz for the configurations studied. The model's pendulum length,  $L$ , was then calculated using Equation 2 where  $g$  is the acceleration due to gravity.

$$L = \frac{g}{(2\pi f_m)^2} \quad (2)$$

The model's initial position was determined by averaging the cropped data set. Next a MATLAB program (Appendix A), based upon one written by Lt Lund [Ref. 11], was written to reduce the raw voltage data from the rangefinder and the controller and to complete error calculations. To convert the voltage data to model displacement in centimeters,  $d$ , Equation 3 was used:

$$d = vpd * 5.12 - \frac{V * vpd * 10.24}{256} \quad (3)$$

Where  $vpd$  is the volts per division setting in the DSO software display,  $V$  is the voltage output from the laser rangefinder,  $d_i$  is the initial displacement of the model in centimeters, 10.24 is the number of divisions displayed and 256 is the number of pixels displayed.

The force required to displace the model was calculated using Equation 4:

$$F = Mg * \tan\left(\arcsin\left(\frac{d - d_i}{L}\right)\right) \quad (4)$$

Where  $M$  is the mass of the model. Equation 4 was used to determine both the MAV's drag and its net thrust at a certain tunnel speed. In order to obtain gross thrust, the drag force required to displace the MAV model was subtracted from the net thrust.

As both the thrust and drag of the MAV vary throughout its flapping cycle, the data reduction program was required to ensure an integer number of cycles were used for its calculations. To accomplish this, the voltage data from the controller was analyzed and cropped as it passed through a certain trigger voltage. One voltage cycle is equivalent to a motor revolution from one positive peak to the next positive peak. One can see from Figure 9 that the controller gives a crisp, repeatable voltage spike for each cycle. As the gearbox has a 25:1 reduction ratio, 25 peaks equate to 1 flapping cycle for the MAV. After the MATLAB program identifies the start of the cycle, it counts the number of times the controller voltage passes through the trigger voltage (on the positive slope) until the 25<sup>th</sup> time when the program calculates the voltage, thrust, and frequency for the flapping cycle.

As three samples of data were taken at each velocity/frequency setting, the means from each sample set were averaged. The reduced data was saved to a summary file for compilation upon completion of the program. The program also allows for a comprehensive summary file for each velocity/frequency setting. This comprehensive summary was useful for trouble shooting during construction of the program.

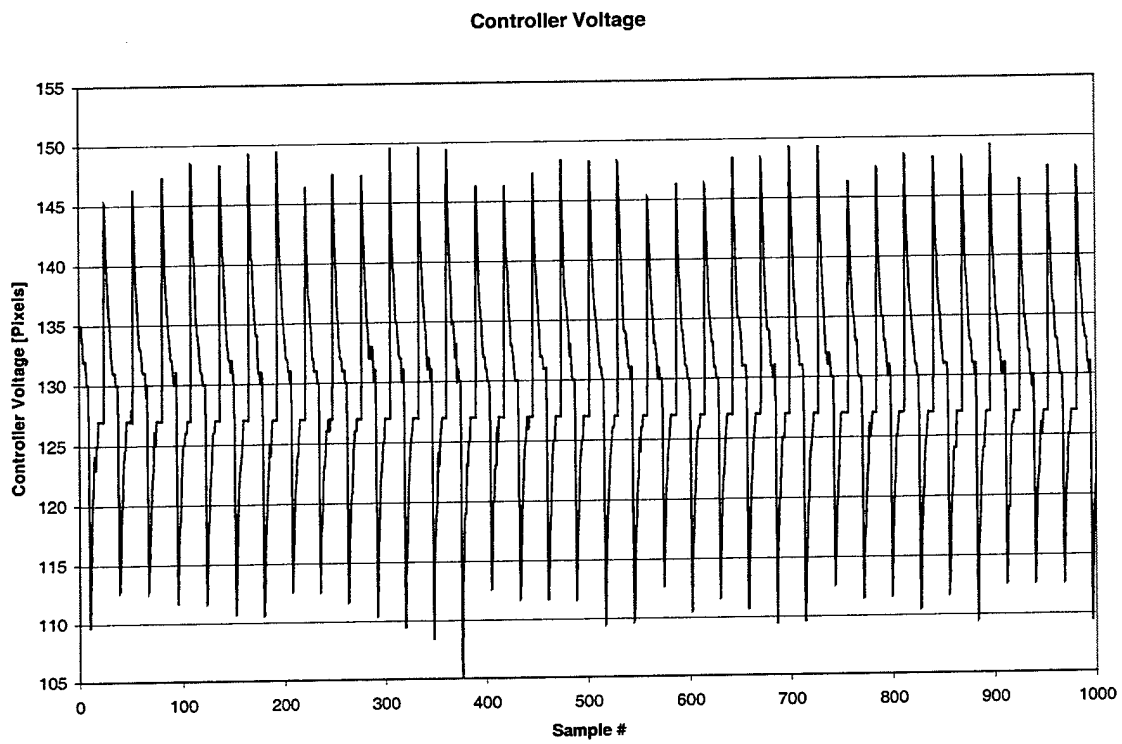


Figure 9. Controller Voltage.

## E. EXPERIMENTAL RESULTS AND ANALYSIS

### 1. Experimental Results

In this paper, the effects of wing mount stiffness on the performance of the flapping-wing MAV were investigated. Four configurations were tested; three with increasing wing mount stiffness and one with an articulated pitch mechanism which attempted to obtain pure airfoil plunge.

In Figures 10 through 13, the thrust obtained from each configuration is plotted versus velocity at approximately 8, 10, 12 and 14 Hz flapping frequency. For three-dimensional plots of the same data, see Appendix B.

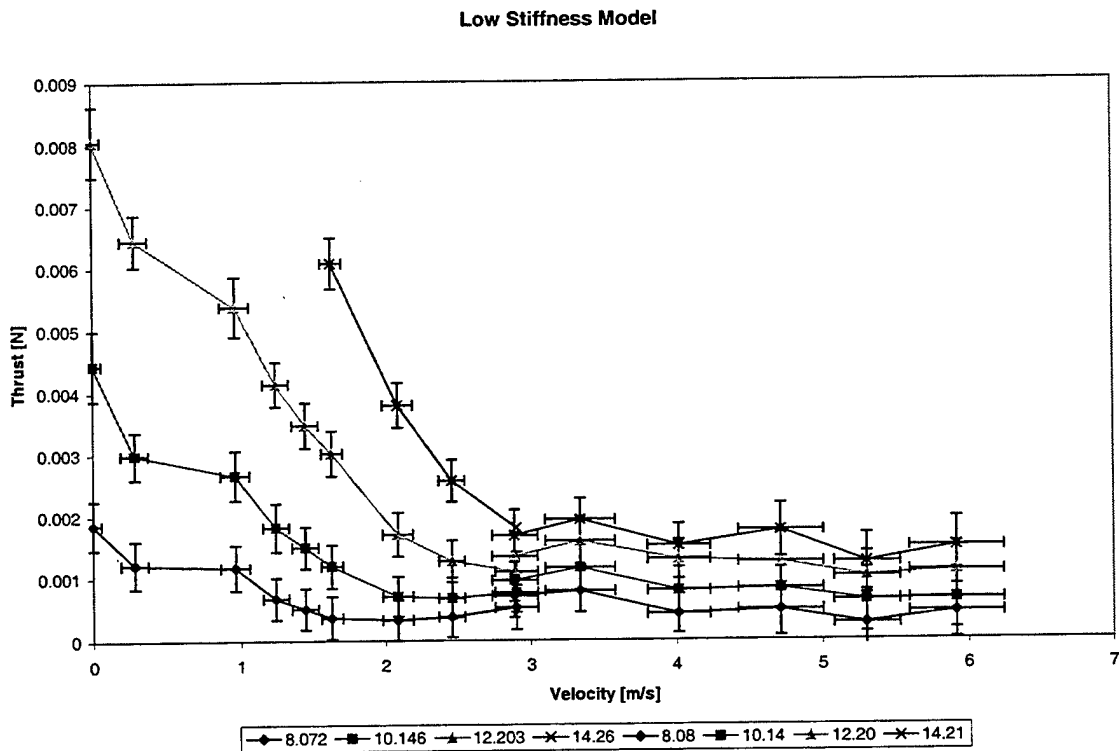


Figure 10. Thrust Performance of Low Stiffness Model.

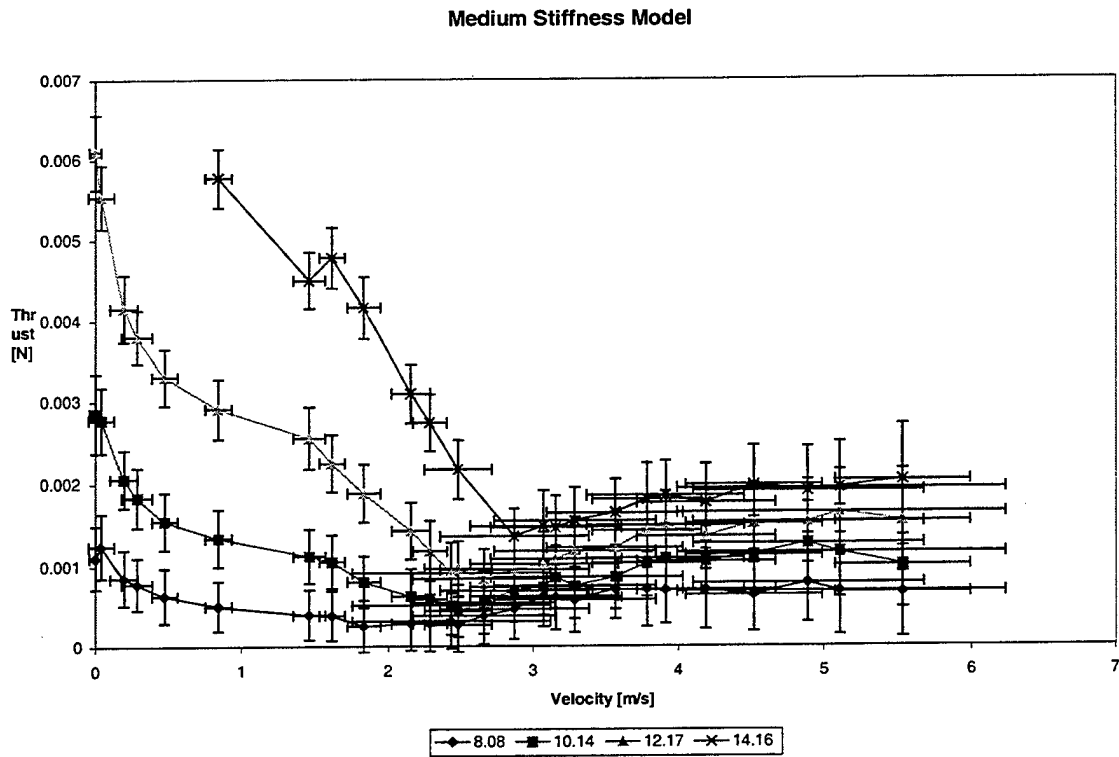


Figure 11. Thrust Performance of Medium Stiffness Model.

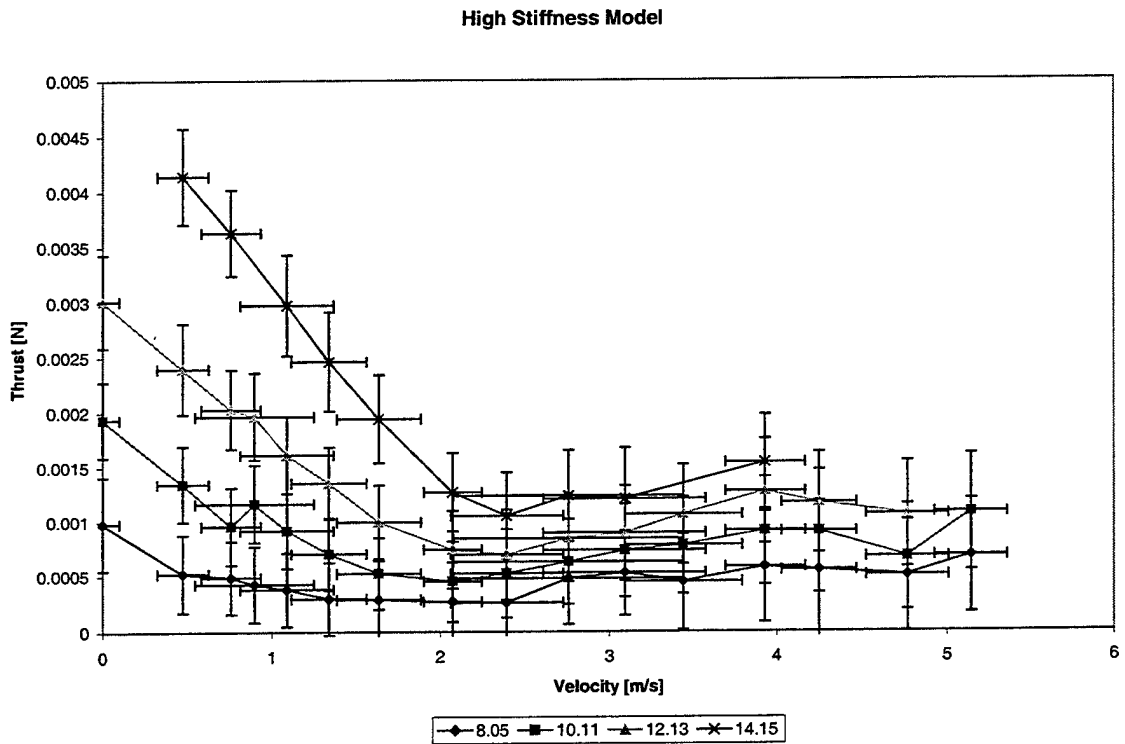


Figure 12. Thrust Performance High Stiffness Model.

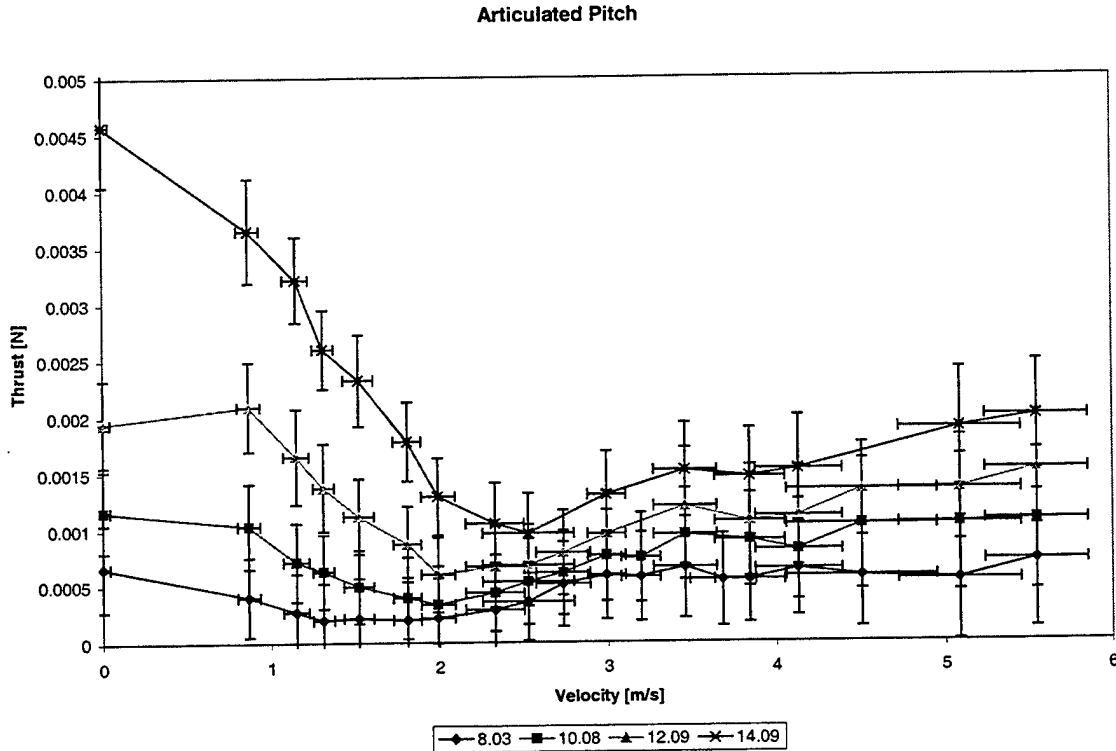


Figure 13. Thrust Performance of Articulated Pitch Model.

From Figures 10 through 13 one can see that the general shape of the thrust vs velocity plot at different frequencies is basically the same for each configuration. Initially, the model produces a high thrust, which quickly reduces to a minimum as velocity increases. When the tunnel speed is further increased, the thrust developed by the model begins to slowly recover. One can see that as the flapping frequency increases, the thrust-velocity lines move upward and to the right for each configuration.

Figures 14 through 17 compare the thrust performance of the four different configurations at each frequency. One can see that in the static case and at extremely low tunnel velocities, the models with the more flexible wing mounts produce greater thrust. The articulated pitch model does not perform well in the static and low speed flow cases. One can see that as the tunnel velocity increases up to the velocity which produces minimum thrust, the thrust performance of the low and medium stiffness models and the high stiffness and articulated pitch models approach each other. Once past the velocity

that produces minimum thrust the performance of the medium stiffness and articulated pitch models surpass that of the high stiffness and low stiffness models.

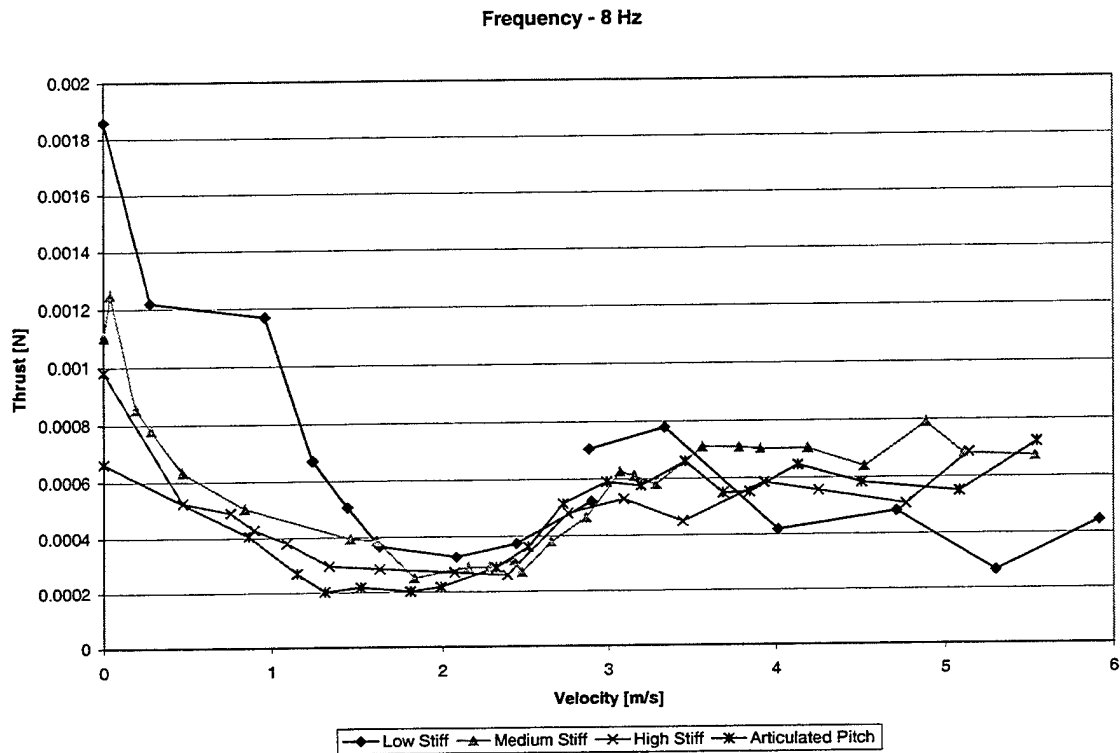


Figure 14. Configuration Thrust Comparison @ 8 Hz.

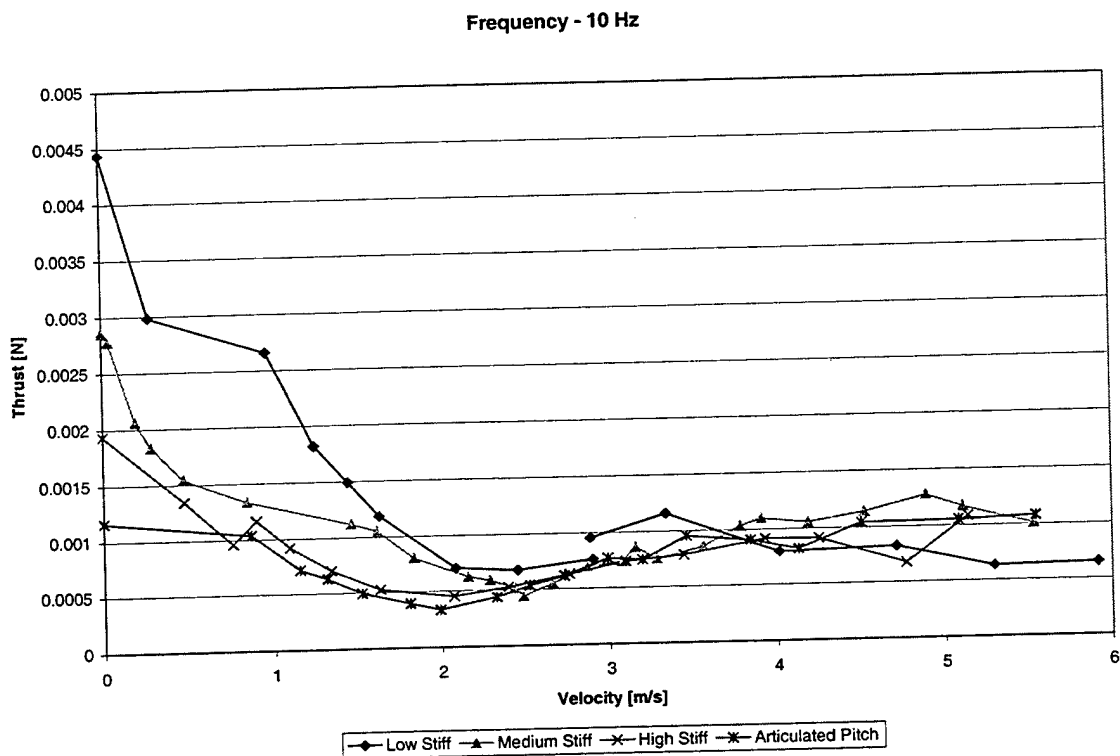


Figure 15. Configuration Thrust Comparison @ 10 Hz.

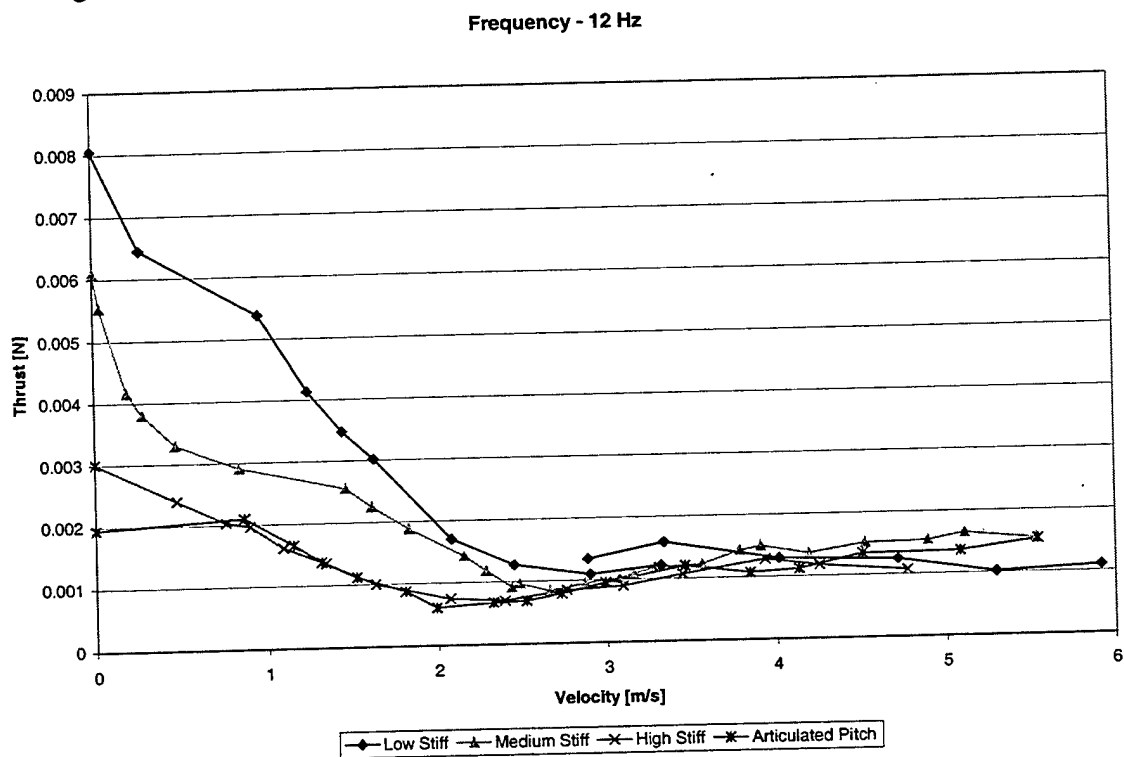


Figure 16. Configuration Thrust Comparison @ 12 Hz.



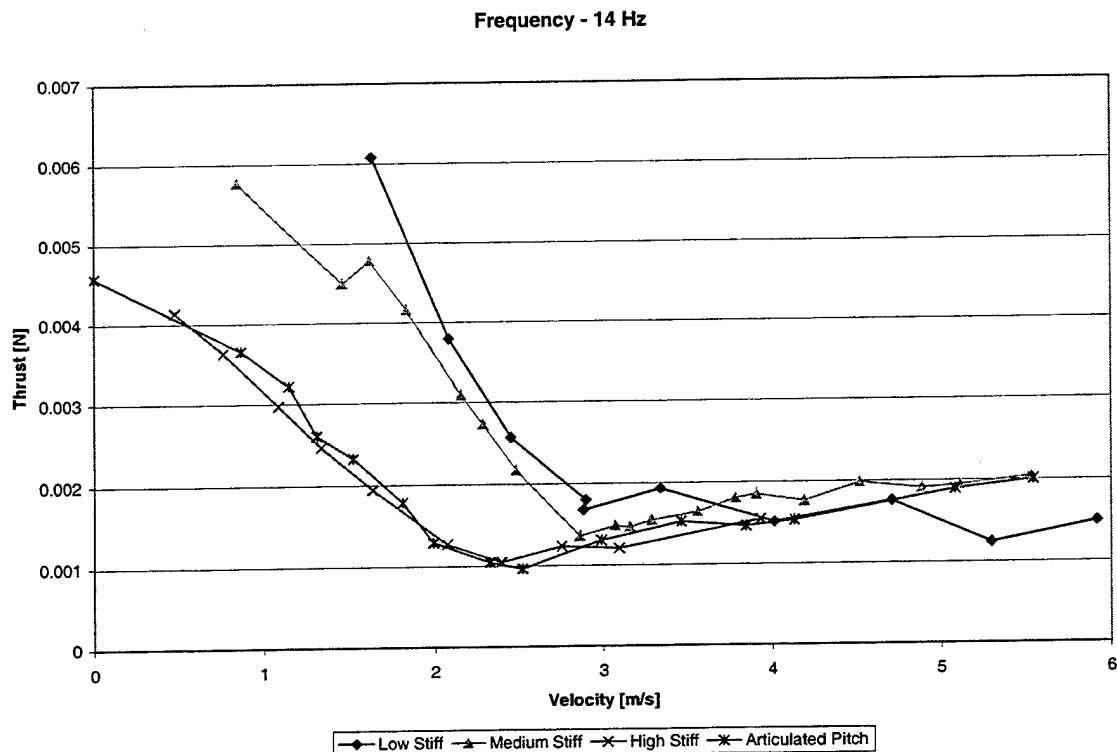


Figure 17. Configuration Thrust Comparison @ 14 Hz.

From the above results, it appears that the best wing mount configuration for a MAV of similar construction to the one used in these tests would be one that had a flexible mount at low velocities and a high stiffness or articulated pitch (pure plunge) mount at higher speeds.

## 2. Error Analysis

There are four primary sources of error associated with the experimental thrust measurements. These four include the error due to the average deviation of thrust between cycles, laser rangefinder error, oscilloscope error, and weight/wire length error. The sum of these four errors is presented as the vertical error bars in Figures 10 through 13. As the in-draft tunnel vents to the atmosphere, the velocity measurements taken by the pitot-static system were highly sensitive to wind conditions. Figures 10 through 13 also illustrate the fact that the velocity error varies greatly day to day. On the days that the data for the low stiffness model was tested, the wind was relatively calm. However,

the second day that the medium stiffness model was tested was extremely windy (> 30mph). The resulting error in velocity was as much as 22%. The velocity error bars displayed in Figures 10 through 13 represent one standard deviation added and subtracted from the mean tunnel velocity.

The first source of thrust error is thrust average deviation. The mean thrust for every complete flapping cycle of the model was calculated. This cycle mean thrust of the model varied from cycle to cycle. This variation was due to a variety of factors but the most significant contributors were that the tunnel intake was indoors and that the outlet vents to the atmosphere. Although the tunnel room was vented to the outside by several banks of windows, the opening and closing of doors and other windows in the building caused slight velocity drift which affected model displacement and thrust. In addition, variations in wind velocity also affected results. Average deviation is similar to standard deviation in that it provides a measure of the width of the data about the mean. It is a more robust estimator, and is given by Equation 5 [Ref. 1].

$$ADev(x_1, \dots, x_N) = \frac{1}{N} \sum_{j=1}^N |x_j - \bar{x}| \quad (5)$$

For this application,  $x$  represents the mean of each cycle,  $j$  is the cycle counter,  $N$  is the total number of cycles, and  $\bar{x}$  is the mean of all cycles. The average deviation was calculated at every frequency and velocity and is considered here to be an estimated error bound. It is the predominant source of error for velocities above approximately 4 m/s.

The second source of thrust error was the laser rangefinder. Rangefinder error consists of a fixed error at the center point (13 cm). A linear error proportional to the distance from the center point is added to the fixed error at all other points. For the ranges encountered here, the rangefinder accuracy is given by the Equation 6:

$$Range\ Error = 0.1mm \pm 0.2\% * Distance\ from\ Center\ Point \quad (6)$$

The third source of thrust error was due to the digital oscilloscope. An error due to the maximum resolution of the oscilloscope was added to all voltage measurements. This error varies with the selected maximum value of the displayed vertical axis. The highest accuracy is obtained when the voltage signal approaches the maximum displayable, but

does not exceed the display window. The oscilloscope accuracy analysis indicated that the actual oscilloscope error was always less than half of its resolution. Statistically, this is reasonable in that errors would tend to occur on both sides of the actual voltage, offsetting each other. In the interest of a conservative analysis, however, the maximum resolution was used as the error. Due to the requirement to capture the maximum displacement of the model at tunnel velocities approaching 6 m/s, the DSO resolution had to be set at 0.5 Volts per division. Consequently, the error associated with DSO resolution was the greatest contributor to thrust error.

The fourth source of error was that associated with the thrust calculations. As discussed in the Experimental Data Reduction section, to determine the thrust produced by the model the weight and length of the model's wires had to be determined. In order to account for the uncertainties in these measurements, a thrust error calculation was carried out using the maximum weight and minimum wire length and was subtracted from the mean thrust for each data set.

### III. FLOW VISUALIZATION

#### A. FLOW VISUALIZATION METHODS

Three methods of flow visibility were used to try and gain insight into the flow field about the MAV. Initially, a smoke rake and fog machine located outside the tunnel intake were used to feed smoke into the test section. Then tell-tale tufts were placed on and around the MAV's wings. Finally a smoke wire smoke system was used to burn fog fluid in the test section near the MAV.

##### 1. Smoke Rake and Fog Machine

Initially, attempts to document the flow field around the MAV were conducted with a smoke rake located just outside the tunnel intake connected to a Rosco 4500 smoke generator by a 25 foot long six-inch ID flexible duct. A smoke rake was constructed with an eight foot-long main tube of six-inch ID, schedule 40 PVC pipe with 16-1.5 inch ID smoke tubes cemented to the main tube. This rake was mounted on a height adjustable stand and can be seen in Figure 18.

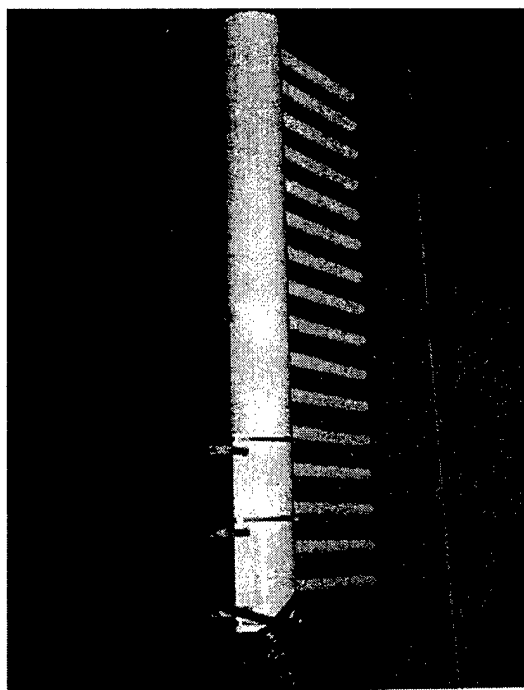


Figure 18. Smoke Rake In Front of Tunnel Inlet.

After several attempts a couple of problems with using the smoke rake located in front of the tunnel intake were discovered. As the fog fluid is burned to generate smoke, it is much warmer than ambient air. Consequently, when the smoke enters the bottom of the rake, it tends to jet past the first few smoke tubes and most of the smoke exits the rake from the top eight tubes. The smoke continued to rise as it entered the tunnel's 9:1 contraction.

In addition, as the smoke passed through the contraction, the smoke stream tubes began to wrap around each other, forming a large spiral of smoke by the time it reached the test section. As the wing span of the MAV was only 150mm and the diameter of the smoke spiral was approximately 30 cm in diameter at the test section, the smoke totally enveloped the MAV and this method was fairly useless for flow visibility purposes. Consequently, other methods of flow visibility were investigated.

## **2. Tell-Tale Tufts**

As Jones [Ref. 10] had some success using single strands of cotton thread (a thread is usually constructed of three or more intertwined strands) glued to the MAV's wings, this method was attempted. To reduce the strand inertia and stiffness problems associated with tufts glued to the wings, single strands of cotton were glued to a balsa wood spar constructed from a MAV wing's leading edge. Even though the strands were not attached to the rapidly flapping-wing, problems with the inertia and stiffness of the fibers were encountered. Once an optimal fiber length was determined (approximately 40 mm) the spar was placed in various positions around the MAV. The best results were obtained with the spar glued to the center rear of the MAV's fuselage with the strands passing between the two flapping-wings.

## **3. Smoke Wire System**

The third method used to document the flow field about the MAV was a smoke wire system. For this method, a bare strand of 0.022" nickel chromium (nichrome) wire was fixed to span the tunnel just ahead of the MAV in the test section. Electrical connectors were attached to the end of the wire on the floor of the tunnel, and on an

adjustable brass tube just above the MAV. The adjustable brass tube also had a port to which a clear silicone tube was attached which delivered fog fluid from a pressurized jug outside the test section. The jug was pressurized using a bike pump through one of two adapters bolted through the jug's cap. The clear silicone tube was attached to the second adapter and fog fluid flow was controlled using a pair of hemostat clamps.

Power for the smoke wire was provided by a Variac set to provide 15-20V. The Variac setting was dependent upon tunnel speed and fog fluid flow rate. The model was installed in the tunnel on a sting that was mounted on a 60 cm span symmetric airfoil that was in turn mounted to a two axis traverse. The flow was illuminated using a Smith-Victor Corp 750W Photographic Light.

Different configurations of the wire were tried to determine the optimum design. Initially, loops were bent in the wire so that the fog fluid would pool there and produce smoke for an extended period. This method did cause the fluid to pool but the loops created significant vortex shedding. Next, 0.005" bare copper wire was tied around the nichrome wire to create longer duration smoke. Vortex shedding was once again observed, however the magnitude was much less than that caused by the looped nichrome wire. The looped wire worked fairly well, however after a few fog cycles, the copper wire knots slid down the nichrome wire. Finally, a straight bare nichrome wire was used. Though some vortex shedding was still observed at higher flow speeds, this configuration gave the most consistent smoke plane. The smoke wire set-up can be seen in Figures 19 and 20.

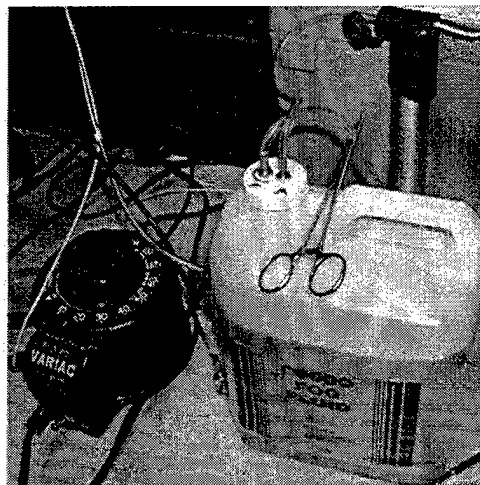


Figure 19. Smoke Wire Set-Up.

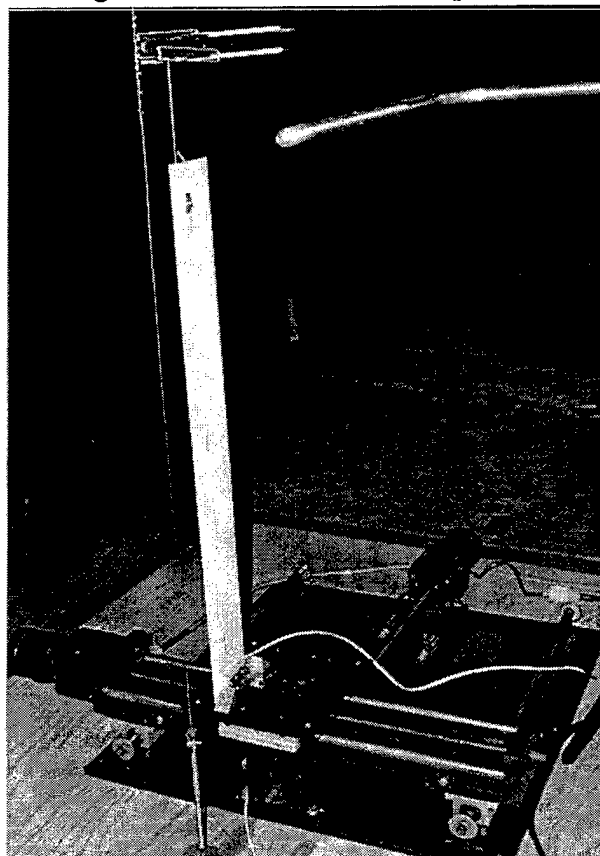


Figure 20. Smoke Wire Set-Up in Tunnel.

Flow images from the smoke wire technique were captured using a Sony DVC-2000 digital video camera and a Kodak DC 260 digital camera. When using the Kodak camera, the focus was manually set at either 24 or 36 inches and the flash was turned on.

## **B. FLOW VISIBILITY RESULTS**

### **1. Tell -Tale Tufts**

Using the tuft method, the best results were obtained when the tuft spar was placed just ahead of the leading-edge plane of the wings mounted on the MAV fuselage. In Figure 21, the medium-stiff winged MAV was flapping at 12 Hz with no wind. The MAV was lit by a strobe light synchronized with the model and the image captured using the Kodak DC 260 digital camera with the focus set manually to 18 inches and the exposure set to 0.5 sec.

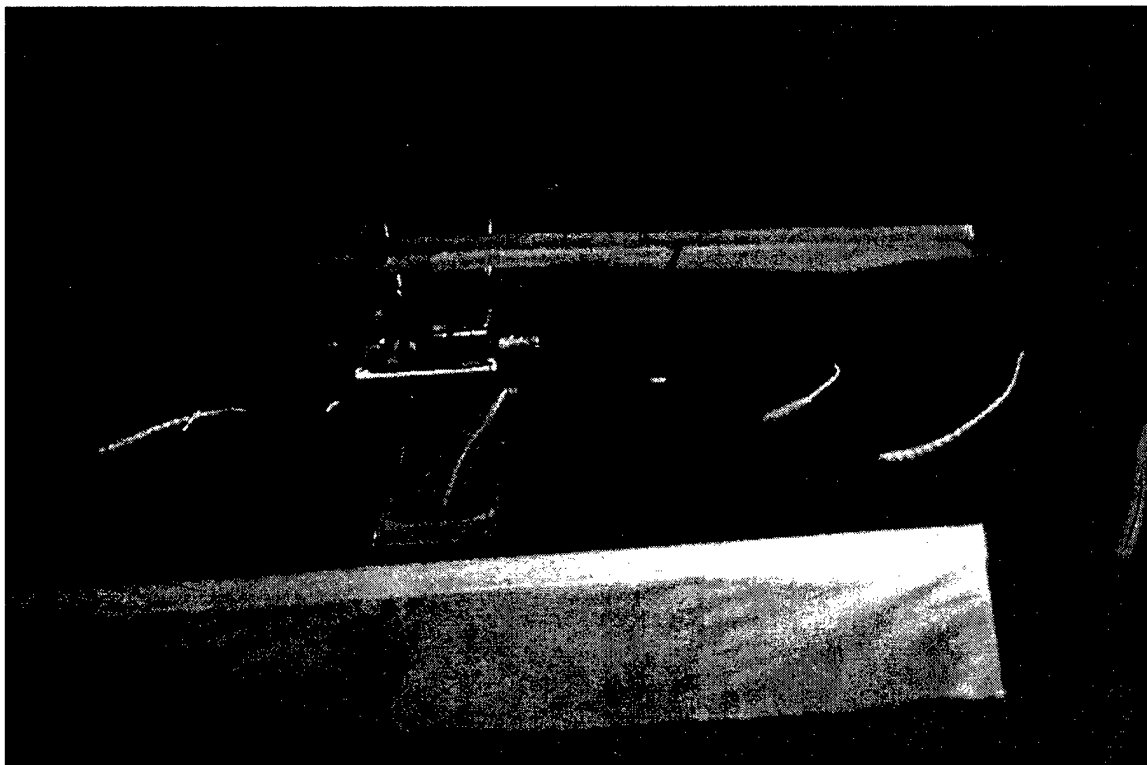


Figure 21. Tell-Tale Tufts, Medium-Stiff Wing, 12Hz Static.

With the given frequency and exposure time, approximately six cycles were captured in this image. This can clearly be seen in the multiple images of the fourth



strand from the right. These multiple images of this strand indicate that the flow between the wings, near the centerline of the MAV is quite unsteady. This image shows the three dimensionality of the flow field around the MAV as the flow is entrained as the wings move apart. Figure 22 illustrates the outward flow from between the wings as they move together. This image is of the MAV with the medium-stiff wing mount, flapping at 12 Hz with flow speed of approximately 2.9 m/s.

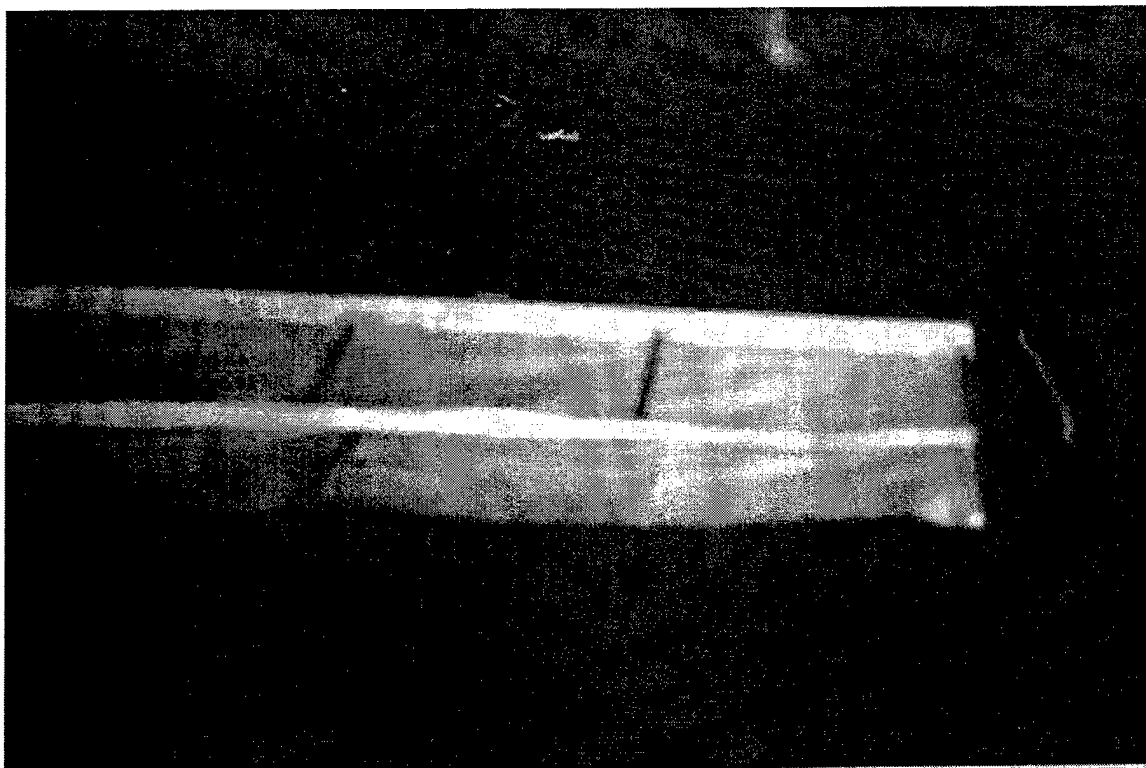


Figure 22. Tell-Tale Tufts, Medium-Stiff Wing, 12Hz, 2.9 m/s Wind Speed.

## **2. Smoke Wire System**

Initially, attempts were made to illuminate the smoke flow using the strobe light. It quickly became clear that the output of the strobe would not be sufficient for capturing smoke images. In addition, as there were no means available to synchronize the camera with the strobe, an exposure length longer than one complete cycle was necessary to ensure that the strobe flash was captured. As the flow around the MAV is unsteady, these attempts to capture an image over more than one cycle lead to significant blurring of the smoke plane. Finally, a Smith-Victor Photographic Light was used to illuminate the flow

and the Kodak DC260's flash was turned on. The images in Figures 23 through 26 were taken from approximately three to four feet downstream of the MAV with the manual focus set to two or three feet.

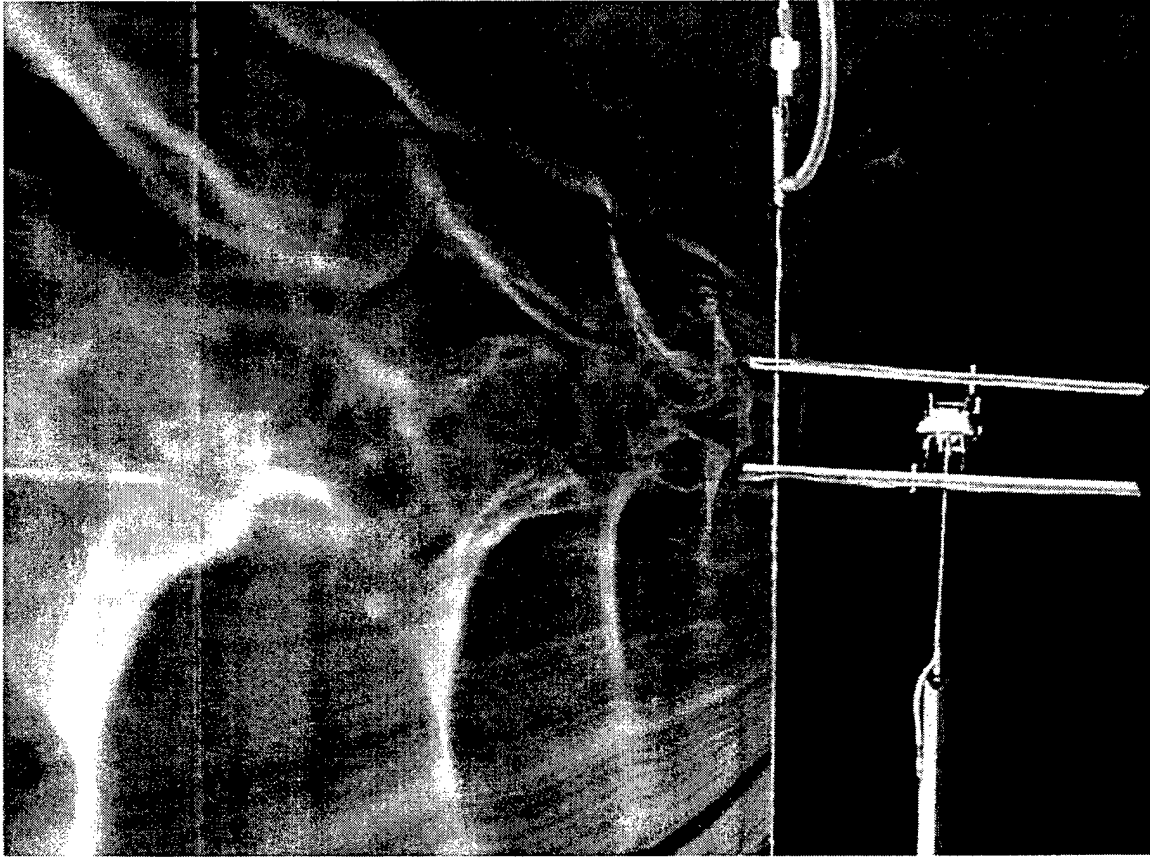


Figure 23. MAV Wing Tip Vortex Induced Wake Structure.

In Figure 23, the smoke wire is positioned approximately six inches upstream of the MAV's port leading edge. One can clearly see the wake structure developed by the wing tip vortices as they are shed during the flapping motion. Looking upstream, as the upper and lower wings move apart, they respectively shed counter-clockwise and clockwise rotating vortices. Correspondingly, when the upper and lower wings move together, they respectively shed clockwise and counter-clockwise rotating vortices. The wing tip vortices can be more clearly observed in Figure 24.

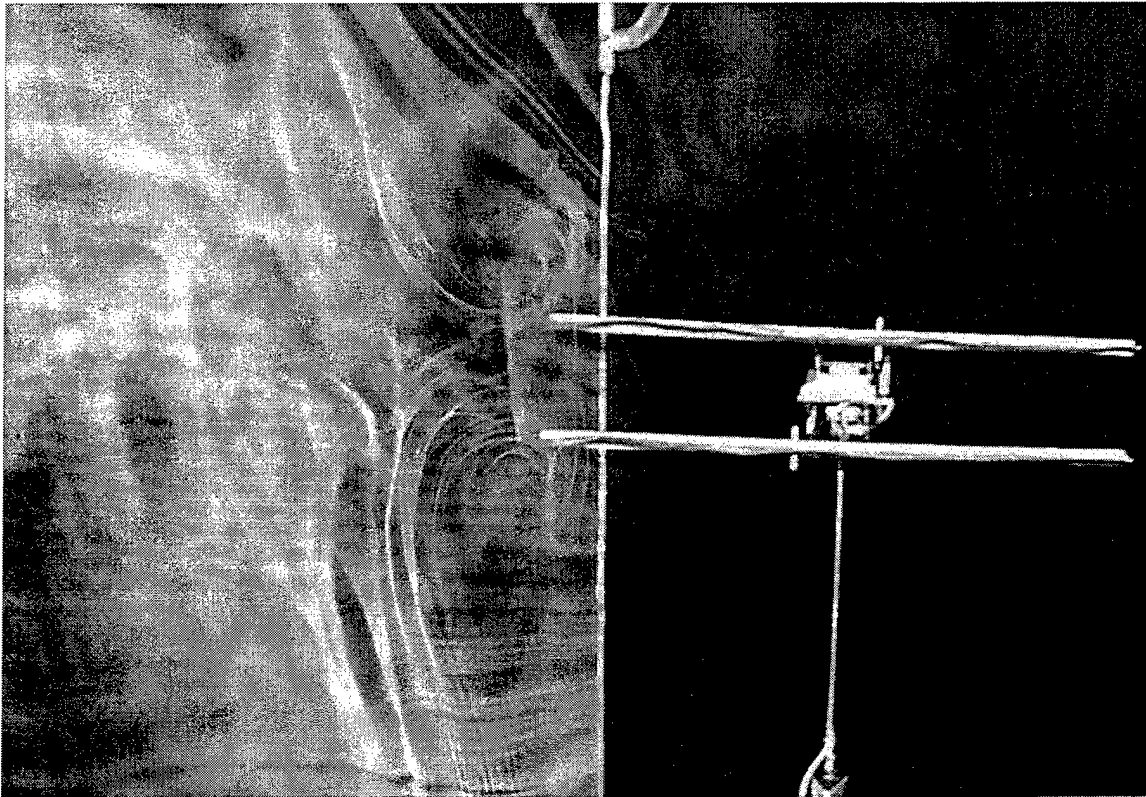


Figure 24. Close Up of MAV Wing Tip Vortices.

The vortices that are clearly visible in Figure 24, were formed as the upper and lower wings moved together. As these vortices grew and coalesced, they formed a jet, which flowed outwards away from the MAV's centerline. The interaction of these vortices also pushed the tip vortices outwards. Once the wings reached their minimum separation, they stopped shedding their vortices and the smoke plane remained flat as can be seen in the vertical smoke line just outboard of the wing tips joining the two vortices. When this image was taken, the MAV's wings had just begun to move apart. The tip vortices which were just forming, are not visible but the effects of the inward flowing jet they formed, can be seen in the deflected smoke plane between the wings to the right of the smoke wire in the image.

The alternating vortices of the upper wing and their effects on the smoke plane can be seen in Figure 25 taken from above and downstream of the MAV. In this image the clockwise rotating vortex nearest the MAV was shed from the upper wing as the wings moved together. The effects of the outward flowing jet created by this vortex set

on the upper portion of the smoke plain can be seen in the deflection of the top of the plain to the left (seen to the left of the vortex in this image).

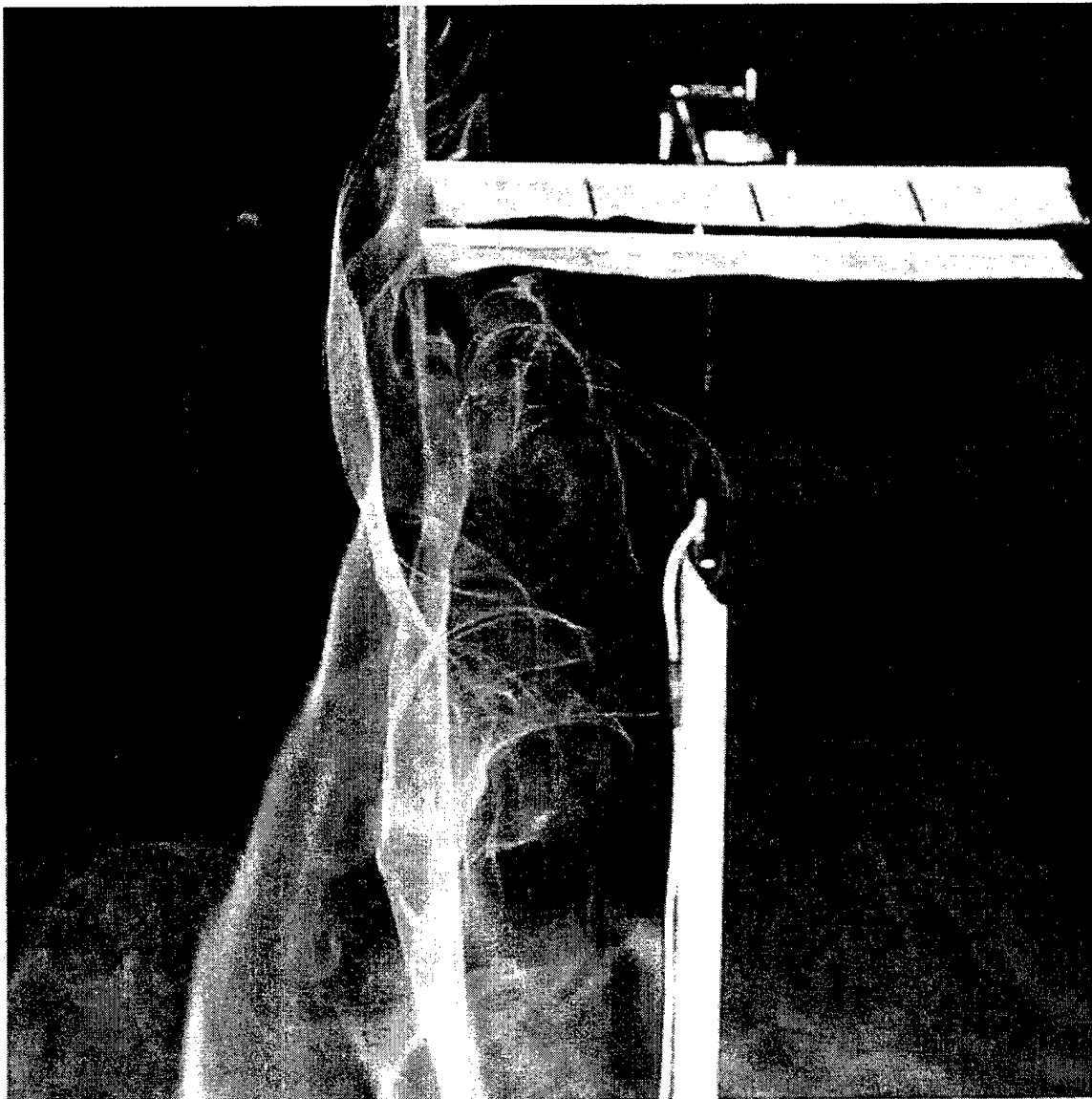


Figure 25. Alternating Vortices Shed from the MAV's Upper Wing.

The second vortex aft of the MAV is counter-clockwise rotating and was shed from the upper wing as the wings moved apart. The effects of the inward flowing jet created by this second vortex set on the upper portion of the smoke plain can be seen in the deflection of the top of the plain to the right (seen above and to the left of this vortex in the image).

The final image obtained by the smoke wire method can be seen in Figure 26. This image was taken with the smoke wire positioned in front of the MAV's nose directly along its centerline. In this image one can see the effects of the boundary layer over the MAV's nose in the upward deflection of the smoke plane. As this image was taken, the wings were at their minimum separation; consequently, the motion of the wings is approaching zero and the smoke plane is relatively undisturbed above the upper wing. Just behind the upper wing, the smoke plane is displaced upwards by the clockwise rotating (as seen from this side of the smoke plane) vortex shed from the upper wing as the wings moved together. As expected in Figure 26, the flow is relatively two dimensional when compared to the flow about the MAV's wing tips.



Figure 26. Two Dimensional Flow Over the MAV's Centerline.

Figures 27 through 35 summarize of the flow field information obtained using the smoke wire system. In Figure 27, the MAV's wings are at their minimum separation and the vortices shed during the closing of the wings have been convected downstream.

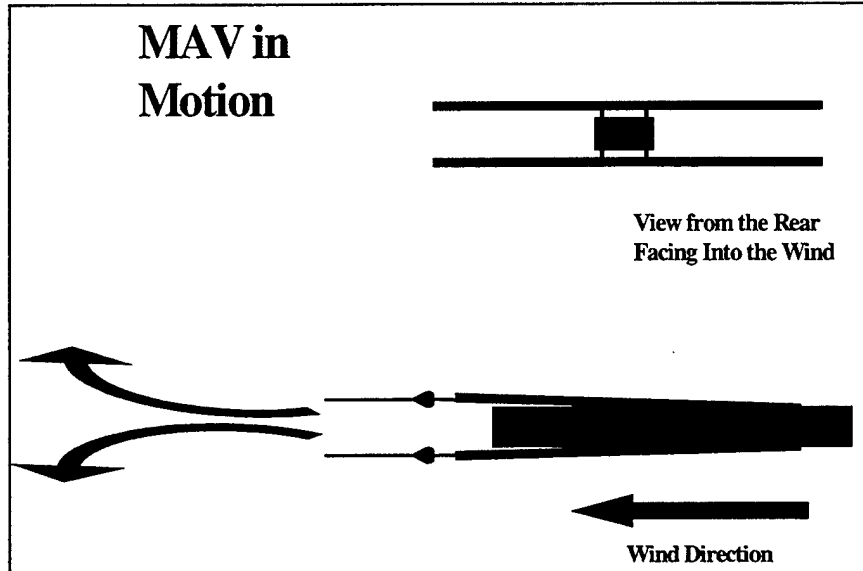


Figure 27. MAV Flow Field – Wings at Min. Separation - Steady.

In Figure 28, the MAV's wings are beginning to move apart. The wings are deflected due to aerodynamic loading and the wings' inertia. Due to the movement of the wings and the resulting change in lift generated by this movement, vortices are formed off the wings' trailing edges and wing tips.

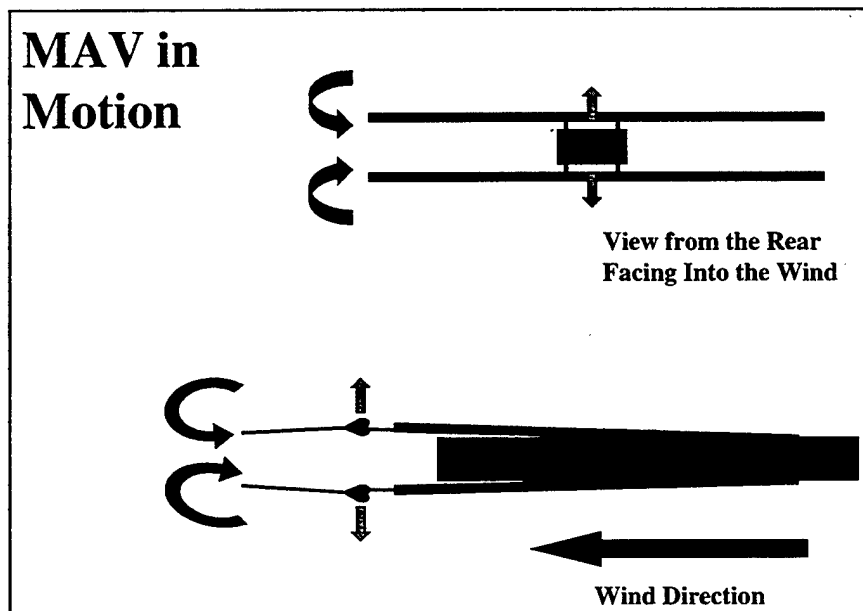


Figure 28. MAV Flow Field – Wings at Min. Separation - Moving.

In Figure 29 the wings have moved apart and accelerated to their maximum plunge speed at their median separation. As the wing tip vortices grow they begin to coalesce and form a jet between them, flowing towards the MAV's centerline. The interaction of the vortices also pushes the vortex pair towards the MAV's centerline. The wind convects the vortices downstream.

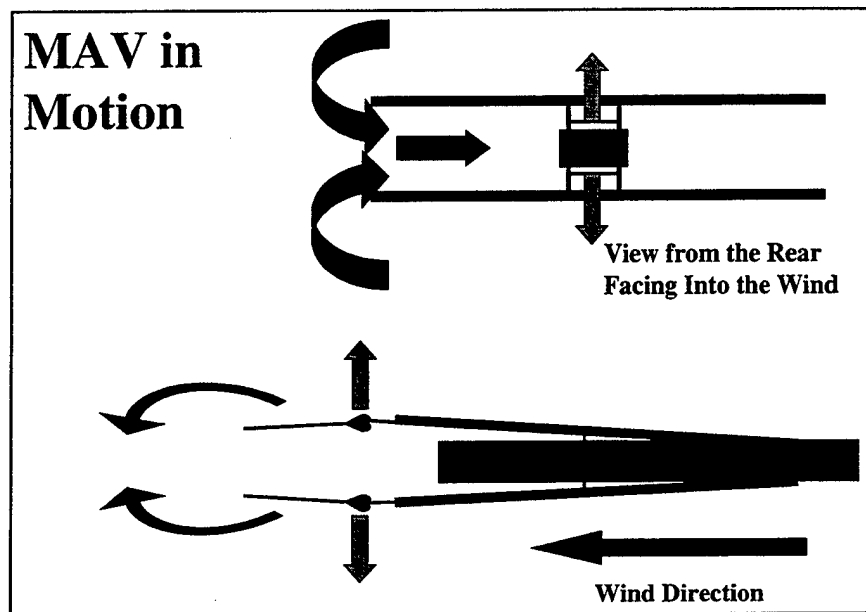


Figure 29. MAV Flow Field – Wings at Median Separation.

In Figure 30 the wings are decelerating as they reach their maximum separation. The intensity of the shedding vortices decreases and they continue to be convected downstream.

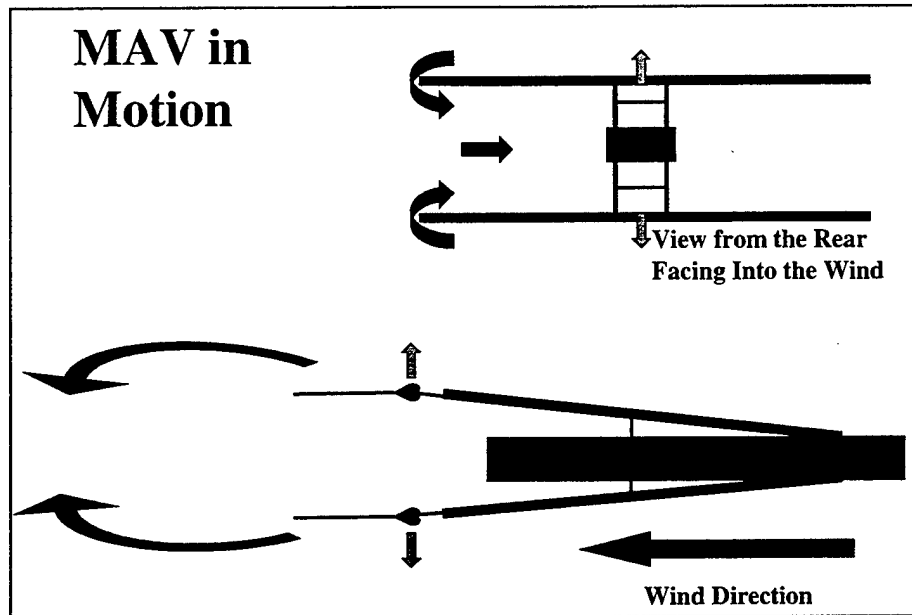


Figure 30. MAV Flow Field – Wings Approaching Max. Separation.

In Figure 31 the MAV's wings are at their maximum separation and are no longer moving. Consequently, the wings cease to shed their vortices.

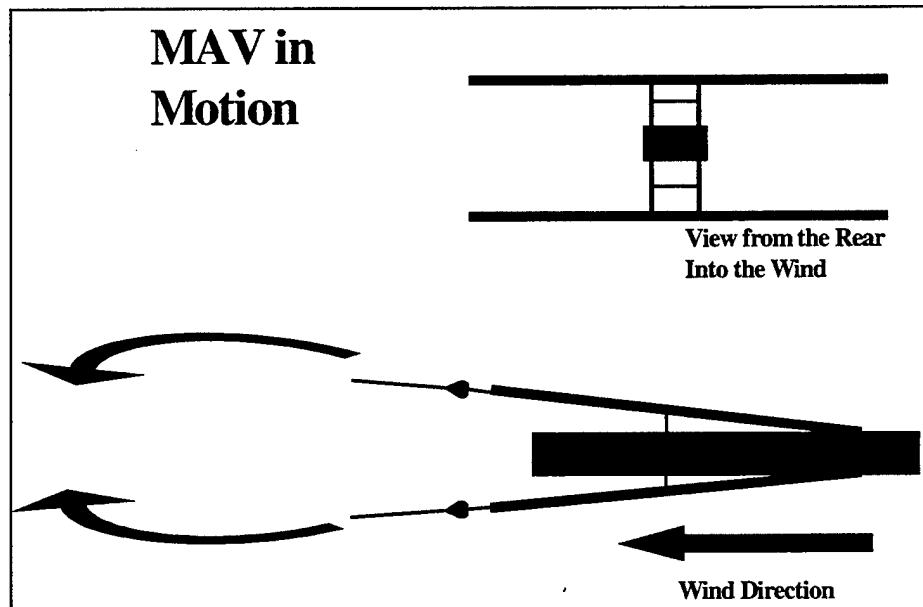


Figure 31. MAV Flow Field – Wings at Max. Separation - Steady.



In Figure 32 the MAV's wings are beginning to move together. One can see that the wings deflect in the opposite direction and the vortices are rotating in the opposite sense to those in Figure 28.

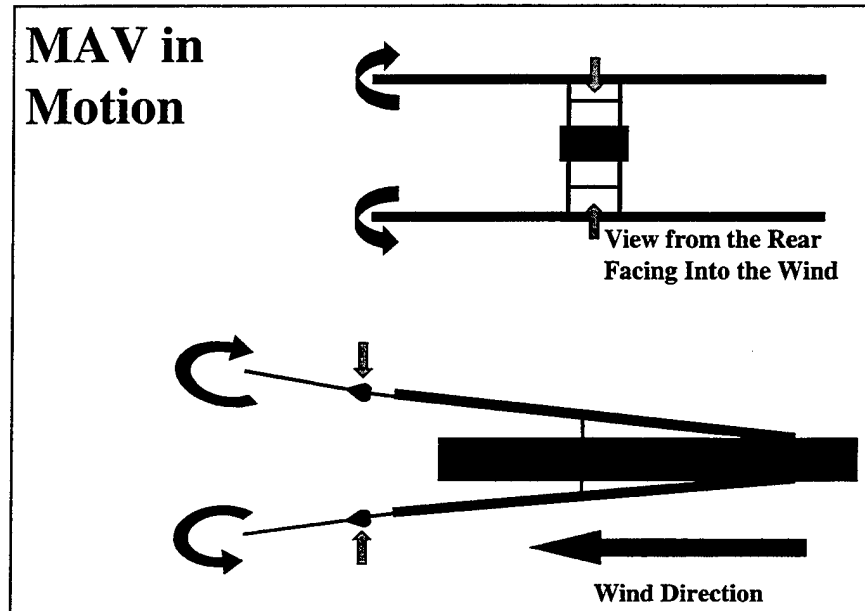


Figure 32. MAV Flow Field – Wings at Max. Separation - Moving.

In Figure 33 the wings have moved apart and accelerated to their maximum plunge speed at their median separation. As the wing tip vortices grow they begin to coalesce and form a jet between them, flowing away from the MAV's centerline. The interaction of the vortices also pushes the vortex pair away from the MAV's centerline. The wind convects the vortices downstream.

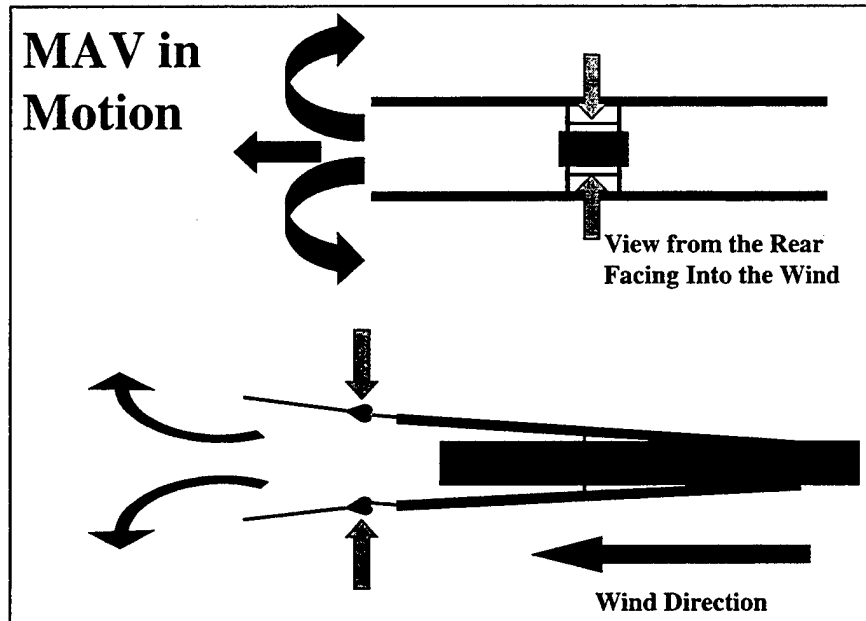


Figure 33. MAV Flow Field – Wings at Median Separation.

In Figure 34 the wings are decelerating as they reach their minimum separation. The intensity of the shedding vortices decreases and they continue to be convected downstream.

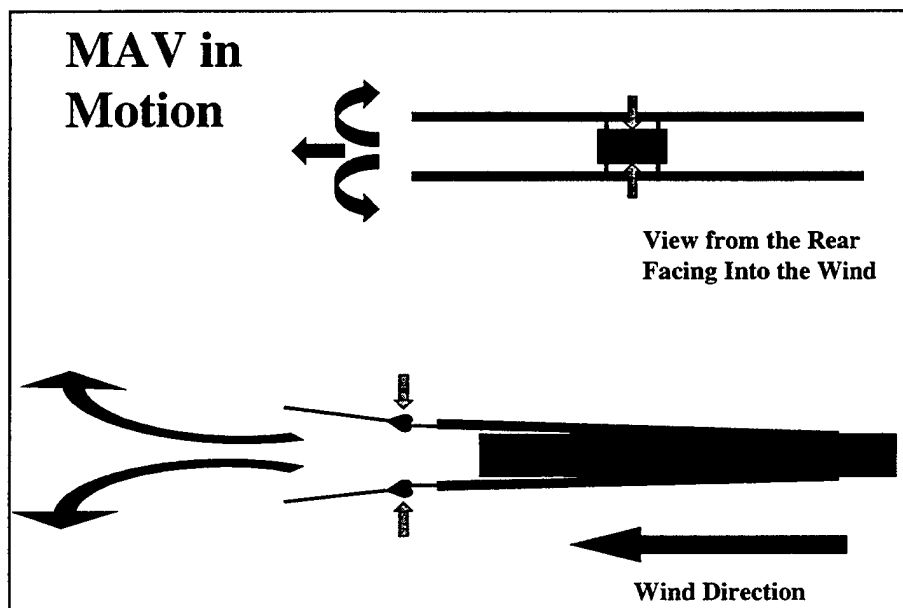


Figure 34. MAV Flow Field – Wings Approaching Min. Separation.

Finally, in Figure 35 the MAV's wings are at their minimum separation and are no longer moving. Consequently, the wings cease to shed their vortices, which have been convected downstream.

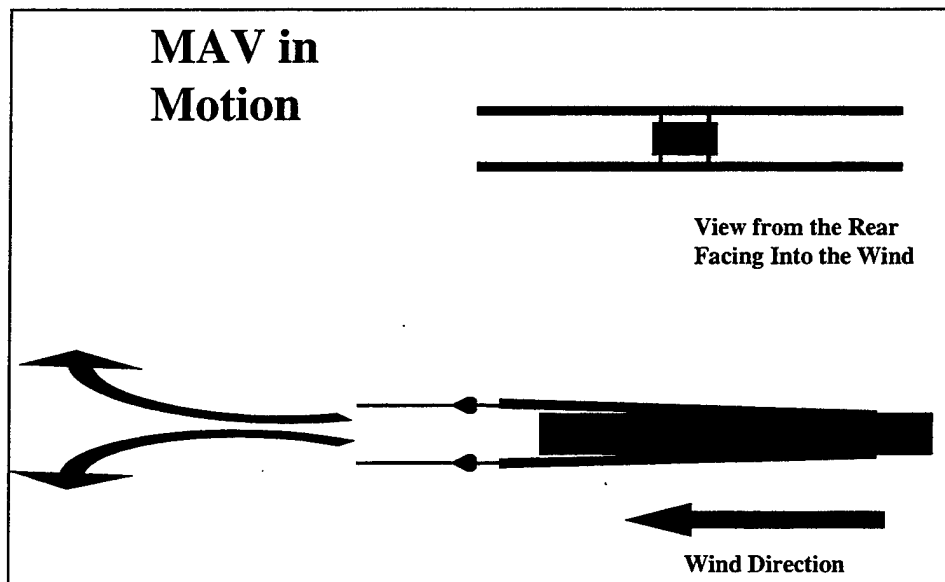


Figure 35. MAV Flow Field – Wings at Min. Separation - Steady.

#### IV. CONCLUSIONS

With a shift towards more diverse military operations in recent years, an operational need for locally owned and operated reconnaissance assets has been identified. The recent development of new technologies has made the construction of small airborne reconnaissance vehicles viable. Nature hints that flapping wings are efficient at the low Reynolds numbers in which these MAVs would operate. Consequently, the potential efficiency of flapping wings as a means of MAV propulsion makes investigation worthwhile.

Experimental testing of a previously constructed MAV was conducted in the NPS 1.5 m x 1.5 m in-draft wind tunnel. For this paper, four different wing configurations were investigated; three with varying degrees of wing mount stiffness and one with an articulated pitch mechanism which attempted to obtain a pure-plunge motion for the wings. Thrust was indirectly determined by measuring the stream-wise displacement of the suspended model due to flapping. The steady-state drag was subtracted from the computed thrust in order to isolate the thrust performance of the MAV and minimize viscous boundary-layer drag effects.

After collection, reduction and analysis of experimental data, it became apparent that in order to optimize the thrust performance of a MAV some sort of active pitch control would be beneficial. At low flow speeds, a flexible wing would produce more thrust, while at higher speeds a stiffer mount or active pitch control to approach a pure plunge motion would be more effective.

Images collected using the smoke wire method were extremely beneficial in determining characteristics of the flow field about the MAV. Further flow visibility efforts need to be made at different flapping frequencies and tunnel velocities so that the flow mechanics responsible for the changing thrust performance can be better understood.

THIS PAGE INTENTIONALLY LEFT BLANK

## **V. RECOMMENDATIONS**

In order to move forward in the development of the flapping-wing as a propulsion system for MAVs, more effort must be put into visualization of the flow field about the MAV. Initial attempts using the smoke wire system were fairly effective at capturing images, but the method can be improved. First, a constant temperature circuit employed in the smoke wire system would simplify the smoke generating process. Secondly, the use of a laser sheet would allow images of the cross section of the wake behind the MAV to be captured. Thirdly, a higher intensity strobe light or multiple synchronized strobes may allow photographic equipment to capture "still" images of the flowfield. This would allow the photographer more control over which portion of the cycle is captured on film. Finally, a flow highlighting system originating from the MAV wing would allow for further investigation into the dynamic stall phenomenon occurring on the MAV wings throughout the flapping process and also highlight the formation of the wing tip vortices. Perhaps the use of titanium tetra-chloride in the in-draft tunnel could be investigated.

THIS PAGE INTENTIONALLY LEFT BLANK

## APPENDIX A. MATLAB PROGRAM FOR DSO-2102 OSCILLOSCOPE DATA REDUCTION

```
%Capt Sean Duggan - MAV / DSO Data Reduction Program
%
%Data Analysis Process:
%- Weigh model with pins before each set of runs (enter weight & max weight [N] below)
%- Install model in tunnel, center laser, swing model to get period data (1 KHz sample
rate)
%- Reduce period data to get wire length [cm], enter below ( $L=(g)/(2*\pi*freq)^2$ )
%- Use period data to determine initial model displacement [pixels], enter below
%
%- Record initial velocity (pressure) data before tunnel on
%- Record velocity at beginning of each run
%- Record final velocity with tunnel off
%NOTE - True velocity=0.4819*(millivolts)^0.489
%       (From LDV / Pitot system calibration from Lt Tim Lund's Thesis)
%
%IMPORTANT: Save data in following format:
%   - freq(100),vel(v000),data set(1 thru 3)
%   - (ie. 100v0001, 100v0002, 100v0003, 101v0001,...,1xxv0003 etc. for each vel)
%   - use freq 100 for drag data (1KHz sample rate)
%   - use freq 101...1xx for thrust data (10KHz sample rate)
%   - take 3 sets of data at each freq/vel setting
%   - save data at each velocity in its own directory (ie. v000, v001, v002...)
%
%- Archive data on CD-R, go to computer with MATLAB to reduce data
%- After data is reduced at each velocity, copy data in Mean_Thrust.wri file to summary
file
%
%NOTES: - If you open Mean_Thrust.wri in EXCEL, copy data to summary file then close
%         Mean_Thrust.wri. If you don't close the file, this program will crash when
%         it tries to delete Mean_Thrust.wri file
%
%- When data reduction complete, subtract drag (100vXXXX) from thrust at each vel to get
% corrected thrust
%- Compile velocity data in one summary file
%- Determine avg vel and standard deviation of vel and copy to thrust summary file

clear
clear all
delete H:\docs\Results\Mean_Thrust.wri;
% ***** Fill in this part *****
filelocation='F:\'; % CHANGE FOR EACH COMPUTER - CD Rom drive location
date='17 May 00\'; % CHANGE FOR EACH RUN - Date directory
dirname='v018\'; % CHANGE FOR EACH VELOCITY - Velocity Directory
filename='v018';
filetype='.prn';
startfilenumber=100; % First file number - Drag data (0.1Hz flap)
lastfilenumber=104; % CHANGE FOR EACH VELOCITY - Last file number
voltsperdiv=0.5;
weight=0.21329; % Model weight in Newtons
weight_max=0.21334; % Max weight for error calcs
wire_length=21.8087386; % Cable length in cm
wire_length_min=21.8090208; % Min wire length for error calcs
disp_intial_pix=123.0946956; % Initial displacement at v0 f0 in pixels
disp_initial=(voltsperdiv*5.12)-(disp_intial_pix)*(voltsperdiv*10.24/256);
% *****
fid1 = fopen('H:\docs\Results\Mean_Thrust.wri','w');
fprintf(fid1,'Filename\tVel\tVel\tMean\tCorrected\tTotal Error\t');
fprintf(fid1,'Avg Dev\tLaser\tDSO\tWT Wire\tMean\tAvg Dev\tMin\tMax\n');
fprintf(fid1,'\t\tStd Dev\tThrust\tThrust\t+/-\tError\tError\tError\t');
fprintf(fid1,'Error\tFrequency\tFrequency\tFrequency\tFrequency\n');
fprintf(fid1,'\t[m/s]\t[m/s]\t[N]\t[N]\t[N]\t[N]\t[N]\t[N]\t[N]\t[N]\t');
fprintf(fid1,'[Hz]\t[Hz]\t[Hz]\t[Hz]\n\n');
```



```

fclose(fid1);

for i=startfilenumber:lastfilenumber
    for k=1:3
        clear data % Clears data matrix each iteration
        if i==100
            sample_rate=1000; % Sample rate in Hz fm DSO (0.1Hz flap - Drag)
        else sample_rate=10000; % Sample rate in Hz fm DSO (Thrust)
        end
        % ***** Loads data *****
        disp(['***** Computing ',num2str(i),filename,num2str(k),filetype,' *****'])
        rawdata=load ([filelocation,date,dirname,num2str(i),filename,num2str(k),filetype]);
        if k ==1
            data1(:,1)=rawdata(:,2); % CH B is loaded to data1 col 1
            data1(:,8)=rawdata(:,1); % CH A is loaded to data1 col 8
            % ***** Converts data to voltage and distance (1V=1cm) *****
            data1(:,2)=(voltsperdiv*5.12)-((data1(:,1))*(voltsperdiv*10.24/256));
            data1(:,9)=(voltsperdiv*5.12)-((data1(:,8))*(voltsperdiv*10.24/256));
            % ***** Does Nothing *****
            data1(:,3)=data1(:,2); % Does nothing
            % ***** Converts voltage to Force [N] *****
            data1(:,5)= weight*tan(asin((data1(:,3)-disp_initial)/wire_length));
            % ***** Computes the avg dev of thrust & freq in data *****
            % DSO data variables
            if i==100
                sig_trip = 132; % Min data value from controller (0.1 Hz flap - Drag run)
            else sig_trip = 140; % Min data value from controller (Thrust runs)
            end
            sig_old1 = 257; % sig_old1, 2, and 3 are the 3 data points prior
            sig_old2 = 257; % to the current pt. Use 257 if the trip signal
            sig_old3 = 257; % is neg voltage. Use -1 if trip is a + voltage.
            % Voltage variables
            cycle_volts=0; % Sum of voltage for one cycle
            cycle_mean_volts=0; % Mean volts of one cycle
            volts_sum1=0; % Sum of voltages of all cycles
            % Thrust variables
            cycle_thrust=0; % Sum of thrust for one cycle
            cycle_mean_thrust=0; % Mean thrust of one cycle
            thrust_sum1=0; % Sum of mean thrust of all cycles
            % Frequency variables
            cycle_mean_freq=0; % Mean frequency of one cycle
            freq_sum1=0; % Sum of frequencies of all cycles
            freq1=0; % Variable for min frequency
            x=1; % Min freq counter
            % Counter variables
            nr_cycles1=-1; % Counter for total number of cycles in data
            cycle_data_pts=0; % Number of data pts within one cycle
            total_data_pts1=0; % Number of data pts of all cycles
            y=-1; % Counter to determine cycles (25 trips = 1 cycle)
            data_points1=length(data1(:,1)); % Counts rows of data matrix
            for j=1:data_points1 % Looks at all data points
                if abs(data1(j,2)) > 5
                    error('*** Voltage is outside rangefinder limits (+/- 5V) ***')
                end
                if nr_cycles1 >= 0 % Ignores partial data before 1st cycle
                    cycle_volts = cycle_volts + data1(j-1,2); % Sums cycle volts
                    cycle_thrust = cycle_thrust + data1(j-1,5); % Sums cycle thrust
                    cycle_data_pts=cycle_data_pts+1; % Counts data pts in cycle
                end
                % Is microswitch tripped?
                if data1(j,8)>=sig_trip & sig_old1<sig_trip & ...
                    sig_old2<sig_trip & sig_old3<sig_trip % This assumes a neg
                    % trip voltage. Change >, < signs if trip is a + voltage.
                    y=y+1;
                    if nr_cycles1 == -1
                        nr_cycles1 = 0;
                    end
                end
            end
        end
    end
end

```

```

if y == 25
    nr_cycles1=nr_cycles1+1;    % 25 Pulses/cycle
    y=0;                        % Resets counter
    % Volts
    cycle_mean_volts=cycle_volts/cycle_data_pts; % Cycle mean
    data1(j-1,4)=cycle_mean_volts; % Stores cycle mean volts
    volts_sum1=volts_sum1+cycle_mean_volts; % Sums total volts
    % Thrust
    cycle_mean_thrust=cycle_thrust/cycle_data_pts; % Cycle mean
    data1(j-1,6)=cycle_mean_thrust; % Stores cycle mean thrust
    thrust_sum1=thrust_sum1+cycle_mean_thrust; % Sums tot thrust
    % Frequency
    cycle_mean_freq=sample_rate/cycle_data_pts; % Cycle mean
    data1(j-1,7)=cycle_mean_freq; % Stores cycle mean frequency
    freq_sum1=freq_sum1+cycle_mean_freq; % Sums all cycle freqs
    if data1(j-1,7)>0
        freq1(x) = cycle_mean_freq; % Save nonzero freqs
        x=x+1;
    end
    total_data_pts1=total_data_pts1+cycle_data_pts;
    % Reset variables
    cycle_volts=0; % Reset cycle voltage for new cycle
    cycle_thrust=0; % Reset thrust summation for new cycle
    cycle_freq=0; % Reset freq summation for new cycle
    cycle_data_pts=0; % Reset nr of data pts for new cycle
end
end
sig_old1 = data1(j,8); % Last signal value
if j>=3
    sig_old2 = data1(j-1,8); % The data value before the last one
    sig_old3 = data1(j-2,8); % Three data points back
end
end
end
if k ==2
    data2(:,1)=rawdata(:,2); % CH B is loaded to data1 col 1
    data2(:,8)=rawdata(:,1); % CH A is loaded to data1 col 8
    % ***** Converts data to voltage and distance (1V=1cm) *****
    data2(:,2)=((voltsperdiv*5.12)-((data2(:,1))*(voltsperdiv*10.24/256)));
    data2(:,9)=((voltsperdiv*5.12)-((data2(:,8))*(voltsperdiv*10.24/256)));
    % ***** Does Nothing *****
    data2(:,3)=data2(:,2); % Does nothing
    % ***** Converts voltage to thrust [N] *****
    data2(:,5)= weight*tan(asin((data2(:,3)-disp_initial)/wire_length));
    % ***** Computes the avg dev of thrust & freq in data *****
    % DSO data variables
    if i==100
        sig_trip = 132; % Min data value from controller (0.1 Hz flap - Drag run)
    else sig_trip = 140; % Min data value from controller (Thrust runs)
    end
    sig_old1 = 257; % sig_old1, 2, and 3 are the 3 data points prior
    sig_old2 = 257; % to the current pt. Use 257 if the trip signal
    sig_old3 = 257; % is neg voltage. Use -1 if trip is a + voltage.
    % Voltage variables
    cycle_volts=0; % Sum of voltage for one cycle
    cycle_mean_volts=0; % Mean volts of one cycle
    volts_sum2=0; % Sum of voltages of all cycles
    % Thrust variables
    cycle_thrust=0; % Sum of thrust for one cycle
    cycle_mean_thrust=0; % Mean thrust of one cycle
    thrust_sum2=0; % Sum of mean thrust of all cycles
    % Frequency variables
    cycle_mean_freq=0; % Mean frequency of one cycle
    freq_sum2=0; % Sum of frequencies of all cycles
    freq2=0; % Variable for min frequency
    x=1; % Min freq counter

```

```

% Counter variables
nr_cycles2=-1; % Counter for total number of cycles in data
cycle_data_pts=0; % Number of data pts within one cycle
total_data_pts2=0; % Number of data pts of all cycles
y=-1; % Counter to determine cycles (25 trips = 1 cycle)
data_points2=length(data2(:,1)); % Counts rows of data matrix
for j=1:data_points2 % Looks at all data points
    if abs(data2(j,2)) > 5
        error('*** Voltage is outside rangefinder limits (+/- 5V) ***')
    end
    if nr_cycles2 >= 0 % Ignores partial data before 1st cycle
        cycle_volts = cycle_volts + data2(j-1,2); % Sums cycle volts
        cycle_thrust = cycle_thrust + data2(j-1,5); % Sums cycle thrust
        cycle_data_pts=cycle_data_pts+1; % Counts data pts in cycle
    end
    % Is microswitch tripped?
    if data2(j,8)>=sig_trip & sig_old1<sig_trip & ...
        sig_old2<sig_trip & sig_old3<sig_trip % This assumes a neg
        % trip voltage. Change >, < signs if trip is a + voltage.
        y=y+1;
        if nr_cycles2 == -1
            nr_cycles2 = 0;
        end
        if y == 25
            nr_cycles2=nr_cycles2+1; % 25 Pulses/cycle
            y=0; % Resets counter
            % Volts
            cycle_mean_volts=cycle_volts/cycle_data_pts; % Cycle mean
            data2(j-1,4)=cycle_mean_volts; % Stores cycle mean volts
            volts_sum2=volts_sum2+cycle_mean_volts; % Sums total volts
            % Thrust
            cycle_mean_thrust=cycle_thrust/cycle_data_pts; % Cycle mean
            data2(j-1,6)=cycle_mean_thrust; % Stores cycle mean thrust
            thrust_sum2=thrust_sum2+cycle_mean_thrust; % Sums tot thrust
            % Frequency
            cycle_mean_freq=sample_rate/cycle_data_pts; % Cycle mean
            data2(j-1,7)=cycle_mean_freq; % Stores cycle mean frequency
            freq_sum2=freq_sum2+cycle_mean_freq; % Sums all cycle freqs
            if data2(j-1,7)>0
                freq2(x) = cycle_mean_freq; % Save nonzero freqs
                x=x+1;
            end
            total_data_pts2=total_data_pts2+cycle_data_pts;
            % Reset variables
            cycle_volts=0; % Reset cycle voltage for new cycle
            cycle_thrust=0; % Reset thrust summation for new cycle
            cycle_freq=0; % Reset freq summation for new cycle
            cycle_data_pts=0; % Reset nr of data pts for new cycle
        end
        end
        sig_old1 = data2(j,8); % Last signal value
        if j>=3
            sig_old2 = data2(j-1,8); % The data value before the last one
            sig_old3 = data2(j-2,8); % Three data points back
        end
    end
end

if k == 3
    data3(:,1)=rawdata(:,2); % CH B is loaded to data1 col 1
    data3(:,8)=rawdata(:,1); % CH A is loaded to data1 col 2
    % ***** Converts data to voltage and distance (1V=1cm) *****
    data3(:,2)=((voltsperdiv*5.12)-((data3(:,1))*(voltsperdiv*10.24/256)));
    data3(:,9)=((voltsperdiv*5.12)-((data3(:,8))*(voltsperdiv*10.24/256)));
    % ***** Does Nothing *****
    data3(:,3)=data3(:,2); % Does nothing
    % ***** Converts voltage to thrust [N] *****

```

```

data3(:,5)= weight*tan(asin((data3(:,3)-disp_initial)/wire_length));
% ***** Computes the avg dev of thrust & freq in data *****
% DSO data variables
if i==100
    sig_trip = 132; % Min data value from controller (0.1 Hz flap - Drag run)
else sig_trip = 140; % Min data value from controller (Thrust runs)
end
sig_old1 = 257; % sig_old1, 2, and 3 are the 3 data points prior
sig_old2 = 257; % to the current pt. Use 257 if the trip signal
sig_old3 = 257; % is neg voltage. Use -1 if trip is a + voltage.
% Voltage variables
cycle_volts=0; % Sum of voltage for one cycle
cycle_mean_volts=0; % Mean volts of one cycle
volts_sum3=0; % Sum of voltages of all cycles
% Thrust variables
cycle_thrust=0; % Sum of thrust for one cycle
cycle_mean_thrust=0; % Mean thrust of one cycle
thrust_sum3=0; % Sum of mean thrust of all cycles
% Frequency variables
cycle_mean_freq=0; % Mean frequency of one cycle
freq_sum3=0; % Sum of frequencies of all cycles
freq3=0; % Variable for min frequency
x=1; % Min freq counter
% Counter variables
nr_cycles3=-1; % Counter for total number of cycles in data
cycle_data_pts=0; % Number of data pts within one cycle
total_data_pts3=0; % Number of data pts of all cycles
y=-1; % Counter to determine cycles (25 trips = 1 cycle)
data_points3=length(data3(:,1)); % Counts rows of data matrix
for j=1:data_points3 % Looks at all data points
    if abs(data3(j,2)) > 5
        error('** Voltage is outside rangefinder limits (+/- 5V) **')
    end
    if nr_cycles3 >= 0 % Ignores partial data before 1st cycle
        cycle_volts = cycle_volts + data3(j-1,2); % Sums cycle volts
        cycle_thrust = cycle_thrust + data3(j-1,5); % Sums cycle thrust
        cycle_data_pts=cycle_data_pts+1; % Counts data pts in cycle
    end
    % Is microswitch tripped?
    if data3(j,8)>=sig_trip & sig_old1<sig_trip & ...
        sig_old2<sig_trip & sig_old3<sig_trip % This assumes a neg
        % trip voltage. Change >, < signs if trip is a + voltage.
        y=y+1;
        if nr_cycles3 == -1
            nr_cycles3 = 0;
        end
        if y == 25
            nr_cycles3=nr_cycles3+1; % 25 Pulses/cycle
            y=0; % Resets counter
            % Volts
            cycle_mean_volts=cycle_volts/cycle_data_pts; % Cycle mean
            data3(j-1,4)=cycle_mean_volts; % Stores cycle mean volts
            volts_sum3=volts_sum3+cycle_mean_volts; % Sums total volts
            % Thrust
            cycle_mean_thrust=cycle_thrust/cycle_data_pts; % Cycle mean
            data3(j-1,6)=cycle_mean_thrust; % Stores cycle mean thrust
            thrust_sum3=thrust_sum3+cycle_mean_thrust; % Sums tot thrust
            % Frequency
            cycle_mean_freq=sample_rate/cycle_data_pts; % Cycle mean
            data3(j-1,7)=cycle_mean_freq; % Stores cycle mean frequency
            freq_sum3=freq_sum3+cycle_mean_freq; % Sums all cycle freqs
            if data3(j-1,7)>0
                freq3(x) = cycle_mean_freq; % Save nonzero freqs
                x=x+1;
            end
            total_data_pts3=total_data_pts3+cycle_data_pts;
            % Reset variables

```

```

        cycle_volts=0;      % Reset cycle voltage for new cycle
        cycle_thrust=0;     % Reset thrust summation for new cycle
        cycle_freq=0;       % Reset freq summation for new cycle
        cycle_data_pts=0;  % Reset nr of data pts for new cycle
    end
end
sig_old1 = data3(j,8);     % Last signal value
if j>=3
    sig_old2 = data3(j-1,8); % The data value before the last one
    sig_old3 = data3(j-2,8); % Three data points back
end
end
end
end

% Voltage and frequency calculations:

data=[data1;data2;data3];
total_data_pts=total_data_pts1+total_data_pts2+total_data_pts3;
volts_sum=volts_sum1+volts_sum2+volts_sum3;
freq_sum=freq_sum1+freq_sum2+freq_sum3;
thrust_sum=thrust_sum1+thrust_sum2+thrust_sum3;
nr_cycles=nr_cycles1+nr_cycles2+nr_cycles3;
freq=[freq1 freq2 freq3];
clear data1
clear data2
clear data3
volts_mean=volts_sum/nr_cycles;
if volts_mean==0      % No or very slow flap case, still need data
    volts_mean=mean(data(:,3));
end
inner_sum1=0; % Inner summation for adev of volts
inner_sum2=0; % Inner summation for adev of freq
freq_mean=freq_sum/nr_cycles; % Mean freq of cycles
max_freq=max(freq); % Max cycle freq of all cycles
min_freq=min(freq); % Min cycle freq of all cycles
data_points=length(data(:,1));
for m=1:data_points
    if data(m,6)~=0
        inner_sum1=inner_sum1 + abs(data(m,4)-volts_mean);
        inner_sum2=inner_sum2 + abs(data(m,7)-freq_mean);
    end
end
adev_freq=inner_sum2/nr_cycles; % Avg dev of frequency
% Thrust
thrust_mean=weight*tan(asin((volts_mean-disp_initial)/wire_length)); % Mean thrust of
cycles
% *** There are 4 sources of thrust error:
% *** 1st one is due to cyclic nature of flapping wing thrust: *****
adev_volts=inner_sum1/nr_cycles; % adev fm voltage data
% *** 2nd source of error - laser rangefinder error [mm] *****
if abs(volts_mean) < 3.5
    error_laser = 0.1 + 0.002 * abs(10 * volts_mean);
else
    error_laser = 0.25 + 0.005 * abs(10 * volts_mean);
end
error_laser = error_laser/10; % Convert range error to volts error
% *** Oscilloscope volt max error=resolution of DSO-2102-3rd error *
error_DSO = (voltsperdiv*5.12)/128;
% *** Convert errors fm voltage to thrust [N] error *****
adev_thrust1=weight*tan(asin((adev_volts)/wire_length));
error_thrust2=weight*tan(asin((error_laser)/wire_length));
error_thrust3=weight*tan(asin((error_DSO)/wire_length));
% *** Computes error due to weight and wire length - 4th error: *****
error_thrust4 =weight_max*tan(asin((volts_mean-disp_initial)/wire_length_min))-
thrust_mean;
error_thrust=adev_thrust1+error_thrust2+error_thrust3+error_thrust4;

```



THIS PAGE INTENTIONALLY LEFT BLANK

## APPENDIX B. THREE DIMENSIONAL PLOTS OF EXPERIMENTAL DATA

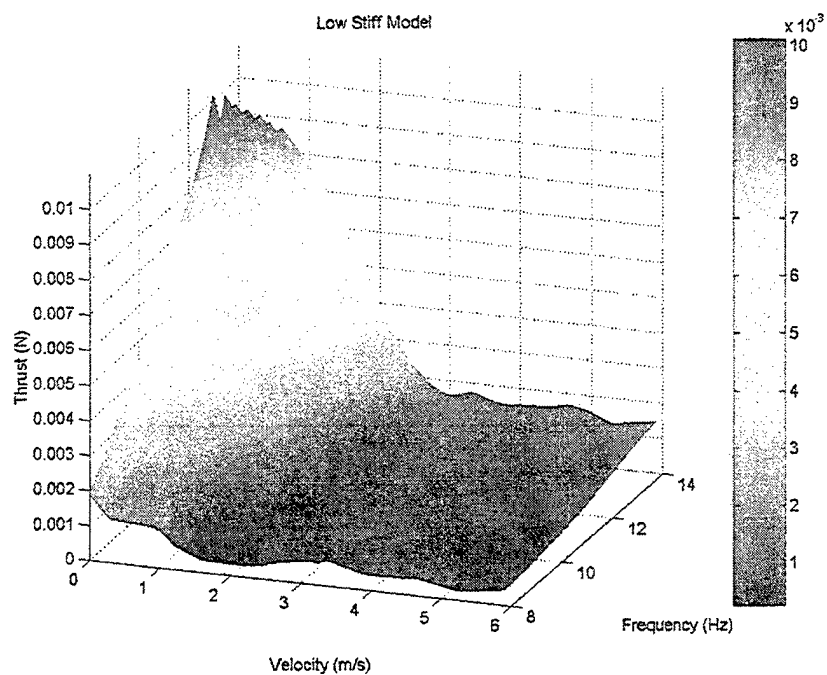


Figure 36. 3-D Plot of Low Stiffness Model's Thrust Performance.

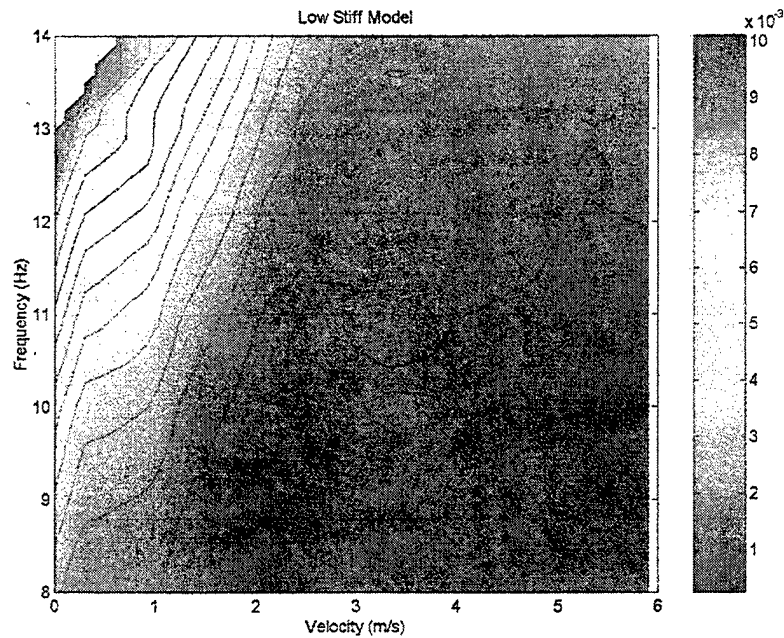


Figure 37. Contour Plot of Low Stiffness Model's Thrust Performance.



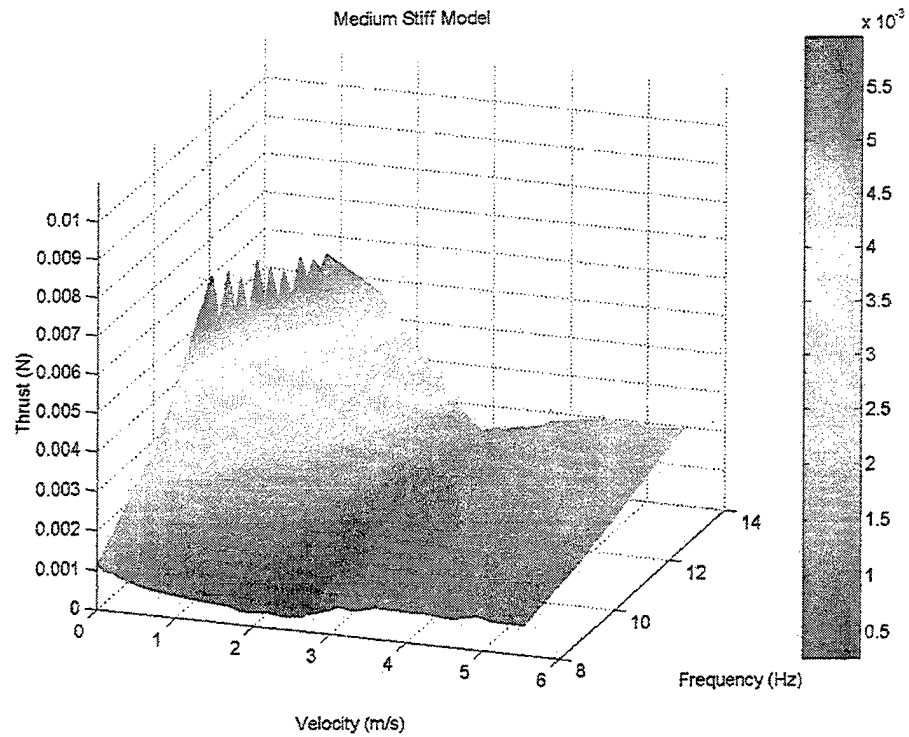


Figure 38. 3-D Plot of Medium Stiffness Model's Thrust Performance.

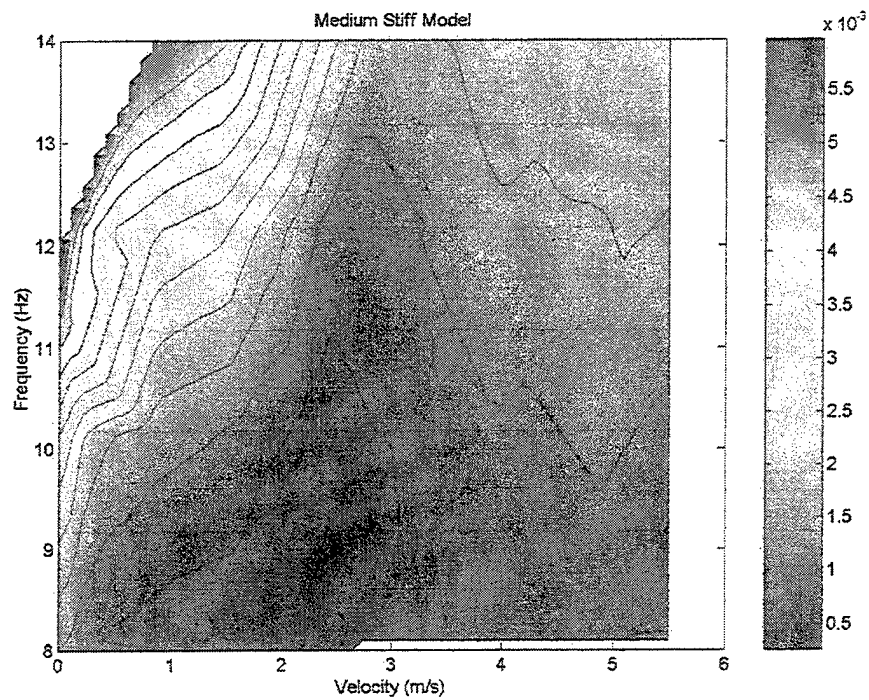


Figure 39. Contour Plot of Medium Stiffness Model's Thrust Performance.

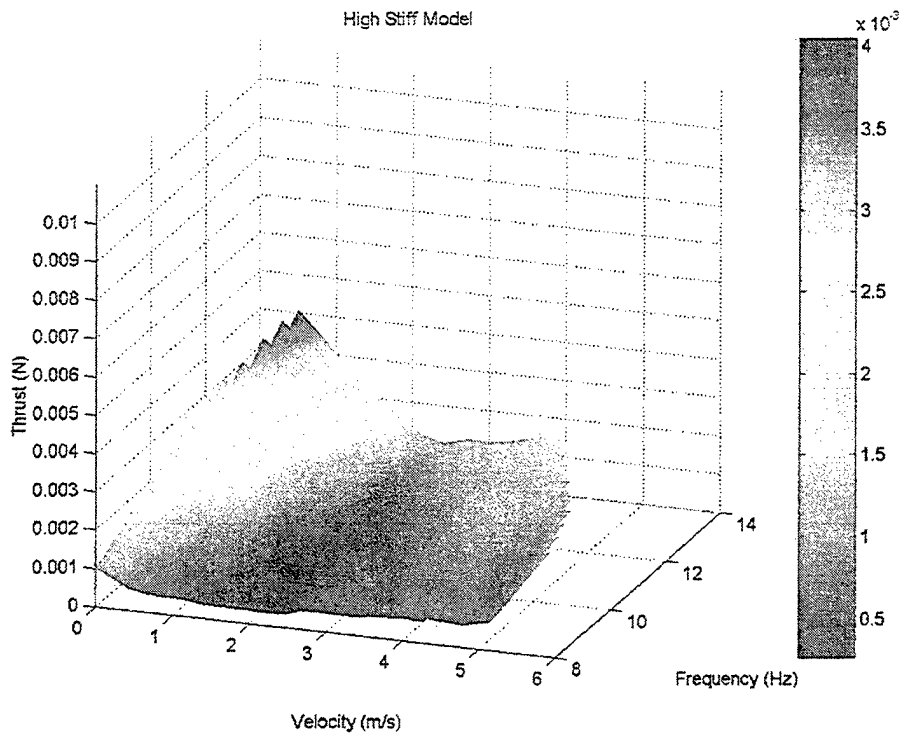


Figure 40. 3-D Plot of High Stiffness Model's Thrust Performance.

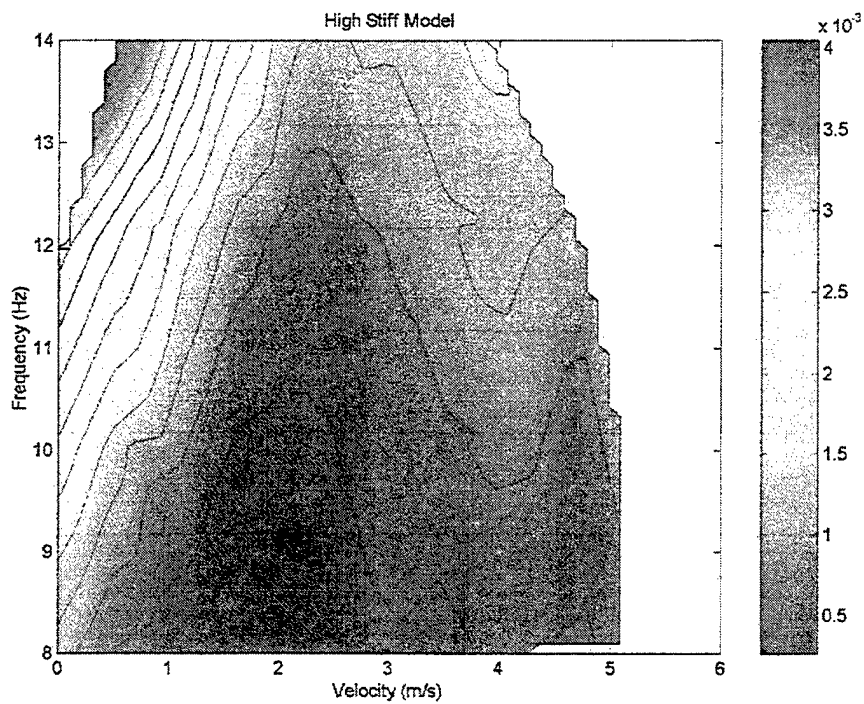


Figure 41. Contour Plot of Medium Stiffness Model's Thrust Performance.

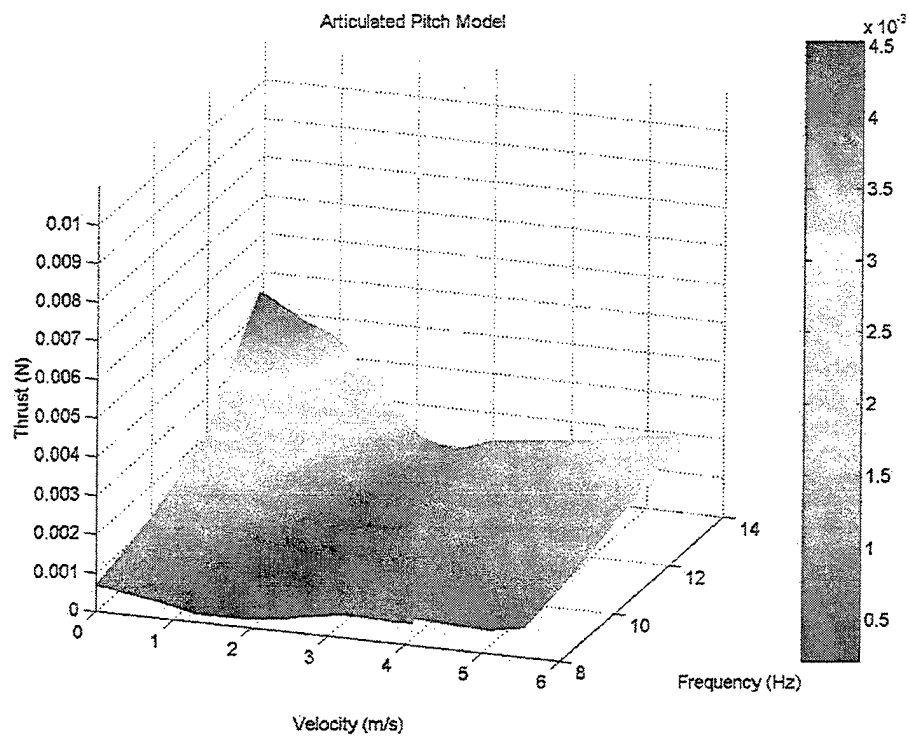


Figure 42. 3-D Plot of Articulated Pitch Model's Thrust Performance.

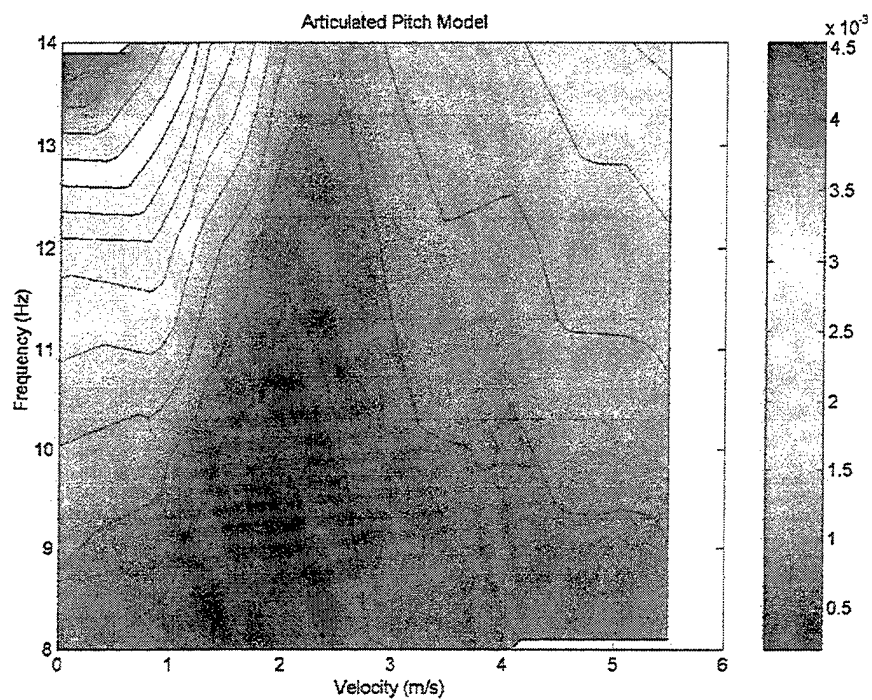


Figure 43. Contour Plot of Medium Stiffness Model's Thrust Performance.

## LIST OF REFERENCES

1. Francis, M. S. and McMichael, J. M., "Micro Air Vehicles – Towards a New Dimension in Flight," [www.darpa.mil/tto/MAV/mav\\_aupsi.htm](http://www.darpa.mil/tto/MAV/mav_aupsi.htm), Aug. 7, 1997.
2. Knoller, R., "Die Gesetze des Luftwiderstandes," *Flug- und Motortechnik* (Wien), Vol. 3, No. 21, 1909, pp. 1-7.
3. Betz, A., "Ein Beitrag zur Erklärung des Segelfluges," *Zeitschrift für Flugtechnik und Motorluftschiffahrt*, Vol. 3, Jan. 1912, pp. 269-272.
4. Katzmayer, R., "Effect of Periodic Changes of Angle of Attack on Behavior of Airfoils," NACA Report No. 147, Oct. 1922 (translated from *Zeitschrift für Flugtechnik und Motorluftschiffahrt*, March 31, 1922, pp. 80-82, and April 13, 1922, pp. 95-101).
5. Birnbaum, W., "Das ebene Problem des schlagenden Flüels," *Zeitschrift für Angewandte Mathematik und Mechanik*, Vol. 4, No. 4, Aug., 1924, pp. 277-292.
6. Birnbaum, W., "Der Schlagflügelpropellor und die kleinen Schwingungen elastisch befestigter Tragflügel," *Zeitschrift für Flugtechnik und Motorluftschiffahrt*, Vol. 15, 1924, pp. 128-134.
7. Von Kármán, T. and Burgers, J. M., "General Aerodynamic Theory – Perfect Fluids," Division E, Vol. II, *Aerodynamic Theory*, Ed. Durand, W. F., 1943, p. 308.
8. Jones, K. D. and Platzer, M. F., "Numerical Computation of Flapping-Wing Propulsion and Power Extraction," AIAA Paper No. 97-0826, Reno, Nevada, January 1997.
9. Jones, K. D. and Platzer, M. F., "An Experimental and Numerical Investigation of Flapping-Wing Propulsion," AIAA Paper No. 99-0995, Reno, Nevada, January 1999.
10. Jones, K. D. and Platzer, M. F., "Flapping-Wing Propulsion for A Micro-Air Vehicle," AIAA Paper No. 2000-0897, Reno, Nevada, January 2000.
11. Lund, T. C., "A Computational and Experimental Investigation of Flapping Wing Propulsion," Master's Thesis, Naval Postgraduate School, Monterey, California, March 2000.
12. Ringleb, F. O., "The Three-Dimensional Smoke Tunnel of the Naval Air Engineering Laboratory in Philadelphia." Report. NAEL-ENG-6818, July 1961.

13. Press, W. H., Flannery B. P., Teukolsky, S. A., Vetterling, W. T., *Numerical Recipes*, Cambridge University Press, 1989, pp. 455, 456.

## INITIAL DISTRIBUTION LIST

1. Defense Technical Information Center ..... 2  
8725 John J. Kingman Rd., Suite 0944  
Ft. Belvoir, VA 22060-6218
  
2. Dudley Knox Library ..... 2  
Naval Postgraduate School  
411 Dyer Rd.  
Monterey, CA 93943-5101
  
3. Dr. Wolfgang Send ..... 1  
DLR – Institute of Aeroelasticity  
Bunsenstr. 10  
D-37073 Göttingen Germany
  
4. Prof. Max F. Platzler, Code AA/Pl ..... 4  
Department of Aeronautics and Astronautics  
Naval Postgraduate School  
Monterey, CA 93943-5000
  
5. Dr. Kevin D. Jones, Code AA/Jo ..... 3  
Department of Aeronautics and Astronautics  
Naval Postgraduate School  
Monterey, CA 93943-5000
  
6. Prof. Dr.-Ing. Dietrich Hummel ..... 1  
Institute of Fluid Mechanics  
Technical University Braunschweig  
Bienroder Weg 3  
D-38106 Braunschweig Germany
  
7. Capt Sean J. Duggan ..... 2  
P.O. Box 4618  
Station Forces Cold Lake, Alberta  
Canada, T9M-2C2